Received: 18 November 2019 | Revised: 12 January 2020 | Accepted: 15 January 2020

DOI: 10.1002/aoc.5573

Applied Organometallic Chemistry WILEY

FULL PAPER

Bis-dioxomolybdenum (VI) oxalyldihydrazone complexes: Synthesis, characterization, DFT studies, catalytic epoxidation potential, molecular modeling and biological evaluations

Mohamed Shaker S. Adam[1,2] | **Mohamed S. Mohamed Ahmed**[1,3] | **Omar M. El-Hady**[2] | **Saad Shaaban**[1,4]

[1]Department of Chemistry, College of Science, King Faisal University, P.O. Box 380 Al-Hofuf, Al-Ahsa, 31982, Saudi Arabia

[2]Chemistry Department, Faculty of Science, Sohag University, Sohag, 82534, Egypt

[3]Chemistry Department, Faculty of Science, Cairo University, Giza, Egypt

[4]Chemistry Department, Faculty of Science, Mansoura University, Mansoura, Egypt

Correspondence
Mohamed Shaker S. Adam and Saad Shaaban, Department of Chemistry, College of Science, King Faisal University, P.O. Box 380 Al-Hofuf, Al-Ahsa 31982, Saudi Arabia.
Email: madam@kfu.edu.sa; shakeradam61@yahoo.com; sibrahim@kfu.edu.sa; dr_saad_chem@mans.edu.eg

Funding information
Deanship of Scientific Research, King Faisal University, Grant/Award Number: 110143

Two *cis-bis*-dioxomolybdenum oxalylsalicylidenedihydrazone complexes (MoO_2L1 and MoO_2L2) were synthesized *via* the complexation of dioxomolybdenum (VI) acetylacetonate with oxalylsalicylidenedihydrazone (H_2L1) and *p*-sodium sulfonate oxalylsalicylidenedihydrazone (H_2L2) *bis*-Schiff base chelating ligands, respectively. The structures of the newly synthesized complexes were confirmed by ^{1}H- and ^{13}C-NMR, IR, ultraviolet–visible and mass spectra, as well as elemental analyses (EA) and conductivity measurements. The spectrophotometric continuous variation method revealed the formation of 2: 1 (metal: ligand molar ratios). DFT studies were applied for the ligands and their Mo-chelates. Interestingly, the *bis*-MoO_2(VI) oxalyldihydrazone complexes showed remarkable catalytic sufficiency towards the selective (ep)oxidation of 1,2-cyclooctene, benzyl alcohol and thiophene using H_2O_2 or *tert*-butyl hydroperoxide (*t*BuOOH) at 85 °C. Under aqueous conditions, the MoO_2L2 (with *p*-sodium sulfonate substituent) exhibited superior that of the MoO_2L1 (without *p*-$NaSO_3$—group), highlighting the role of sodium sulfonate substituent in the catalytic progress of the Mo-chelate. The ligands (H_2L1 and H_2L2) and their corresponding Mo-complexes (MoO_2L1 and MoO_2L2) were assessed for their antitumor and antimicrobial activities. Furthermore, the antioxidant activity was also evaluated using the 2,2-diphenyl-1-picrylhydrazyl (DPPH) and superoxide dismutase (SOD) assays. The binding nature between the Mo-complexes and calf thymus DNA (ctDNA) was also studied within spectroscopic and hydrodynamic techniques.

KEYWORDS
anticancer, antimicrobial, *Bis*-dioxomolybdenum, catalysis

1 | INTRODUCTION

Molybdenum (Mo) is an essential trace element found in several plant enzymes (e.g. nitrogenases and oxidases).[1] The indispensable role of Mo in biological processes was intensively examined in the last decades owing to its interesting redox-catalytic features. The coordination nature around the molybdenum center could not only stabilize various oxidation states of Mo ion in its complexes but also could control its redox properties.[2]

On the other hand, Schiff bases or imines exhibit diverse pharmacological activities, e.g. anticancer, antiparasitic and anti-inflammatory activities.[3] Interestingly, the biological properties of Schiff bases are usually improved after coordination with various transition metal ions.[4] Indeed, Mo-Schiff base complexes would not be of potential interest only in medicinal chemistry but also in homogeneous and heterogeneous catalysis.[5,6] For example, the high affinity of the transition metal-imine pincer chelates to bind ctDNA was used for nucleic acid footprinting.[7] Accumulatly, Abdel-Rahman *et al*.[8,9] reported that the Pd (II), Ag (I), and Cu (II) chlorobenzylidene Schiff base complexes and the Ni (II), Mg (II), Cr (III), and V (II) imine complexes exhibited good anticancer activity.[8,9] Furthermore, oxide- and/or dioxide-vanadium imine complexes were reported as protein-tyrosine phosphatase 1B inhibitors[10,11] and represented as ctDNA cleaving reagents.[12] Additionally, several imine-based complexes of Cr^{2+}, Fe^{2+}, Mn^{2+}, Cu^{2+}, Cd^{2+}, $Co^{2+,}$ and Ni^{2+} ions manifested high interesting antimicrobial and anticancer activities.[13–16]

The chemistry and biology of aroyl hydrazones of alternative aldehydes or ketones as metal-complexes continue to accept much attention in research due to their structural attractive features.[17] Aroyl hydrazine complexes were incorporated in zeolite as heterogeneous catalysts for the degradation of industrial wastewater.[18]

Dihydrazones are the most common chelating ligands for the coordination with transition metal ions of different oxidation states. In this context, aroyldihydrazones, specifically oxalyldihydrazones, are stereochemically and geometrically reactive,[19] providing highly stable metal complexes of wide applications in different scientific areas (e.g. biological chemosensors[20,21] and organic photovoltaic materials[22,23]). Alternative metal-dihydrazones pincer chelates reported good anticancer and antimicrobial activities owing to their ctDNA binding capability and cleavage imperatively.[24]

On the other hand, catalytic (ep)oxidation of olefins, alcohols or thiophenes is still challenging in the synthesis of pharmaceuticals and fine chemicals.[25] Epoxides, aldehydes or ketones in this context are important synthetic intermediates, which employed for the preparation of different industrial materials and petrochemicals, such as paints, epoxy resins and surfactants.[26] Industrially, transition metal-based catalytic (ep)oxidation of alkenes under mild conditions has recently gained great interest.[27,28] (Ep)oxidation of alkenes and alcohols catalyzed by Mo (VI)-complexes was intensively studied in recent years.[4,29] $Mo^{VI}O_2$-complexes are routinely used in the production of industrial propylene oxide and in the efficient chemoselective oxidation of linear and branched alkenes.[29–33] Recently, the molybdenum (VI) complex of picolinic acid-based metallomicellar catalyst was used in the controlled and chemoselective oxidation of the activated alcohols in the aqueous medium, which afforded high sufficiency.[34] Supported dioxomolybdenum (VI) complex of Schiff base on Merrifield resin assigned high selectivity in the oxidation of primary and secondary alcohols by H_2O_2.[35] An interesting metathetic oxidation of 2-butene to acetaldehyde by O_2 gas catalyzed by the immobilized MoO_2-hydrazone complexes on SiO_2, heterogeneously, afforded high yields.[36] The heterogeneous molybdenum-salicylidene 2-picoloyl hydrazone complex, which supported on Fe_3O_4 nano-particles, showed high catalytic potential in the (ep)oxidation of various olefins.[37] Molybdenum acetylacetonate complexes, which supported on functionalized boehmite nano-particles, investigated as catalysts in the (ep)oxidation of unsaturated hydrocarbons presenting high potential.[38] Dioxido-molybdenum (VI) complexes as robust and highly efficient precatalysts for alkene (ep)oxidation, were investigated recently by Mösch-Zanetti *et al*.[39] The catalytic activity of chiral molybdenum (VI) complexes with tridentate Schiff bases derives was evaluated in the oxidation of prochiral sulfides and olefins.[40] Homogeneously, the homobinuclear molybdenum *bis*-oxazoline complex displayed high activity in the oxidation of alkenes and sulfides.[41] Under the organic solvent-free condition, as one of the most favored for the eco-friendly condition in the oxidation protocols, recent efficient and selective oxidation of alcohols with *t*BuOOH catalyzed by a $(MoO_2)^{2+}$-Schiff base complex was examined by Hatefi-Ardakani *et al*.[42] Such condition attacked also the catalytic oxidation of olefins by *t*BuOOH and catalyzed by dinuclear oxomolybdic complexes of salicylideneaminophenolate and -aminoethanolato ligands with alternative catalytic sufficiency of the Mo-catalysts.[43]

The high efficient catalytic and chemoselective properties of *cis*-(MoO_2)-complexes have therefore attracted our attention to design novel class of MoO_2(VI)-complexes based on the use of readily available yet cheap ligands, *e.g.* oxalyldihydrazone ligands.

Herein we report the preparation, characterization and molecular modeling of two *cis-bis*-dioxomolybdenum (II) oxalyldihydrazone complexes. Different physicchemical and spectroscopic techniques are applied for the characterization of the newly synthesized complexes. Their catalytic potentials are examined in different (ep) oxidation substrates, *e.g.* 1,2- cyclooctene, benzyl alcohol and thiophene. Furthermore, the anticancer and microbial activities of the ligands (H_2L1 and H_2L2) and their corresponding Mo-complexes (MoO_2L1 and MoO_2L2) are evaluated against different cancer cell lines and pathogenic microbial strains. Moreover, their antioxidant properties are also assessed using DPPH and SOD assays. Their characteristics binding to ctDNA are investigated within different methods (spectrophotometry and viscosity measurements) considering their combination with ctDNA.

2 | EXPERIMENTAL

2.1 | Reagents and methodology

All starting materials, which are necessary for all chemical reactions and biological studies, ordered from Across, Fluka and Sigma-Aldrich. They have been assigned in all chemical processing systems without any treatment. Percentages of main elements, C, H and N in their compounds were evaluated by GMBH VarioEl model V2.3 CHNS apparatus. The nuclear paramagnetic resonance spectrum for H and C-atoms was determined using Bruker ARX400 multinuclear NMR spectrometer for ^{1}H-nuclei at 400.1 Hz and for ^{13}C-nucleus at 100.6 MHz at ambient temperature. Chemical shifts, δ, of ^{1}H-nuclei and ^{13}C-nucleus were accomplished in ppm. Coupling constant data (J) of neighbors ^{1}H-nuclei in were given by Hz, hertz, as J_{HH}. Ultraviolet and visible spectrophotometry for the studied compounds was estimated using Jasco Ultra violet-Visible spectrophotometric apparatus (model V-570) within a 10 mm silica cell at room temperature by using a thermostatted cell holder. IR-stretching spectral scans were measured from 4000 to 400 wavenumbers (cm^{-1}), as KBr discs, by using Shimadzu FTIR-8101 Fourier Transform Infrared Spectrophotometer. Determination of conductivity measurements of the studied complexes was achieved by Jenway conductometer of model 4320, contacted with an epoxy bodied conductivity cell, as two electrodes. At 25 °C, calibration of the cell constant was taken place from 0.01 to 19.99 of the conductometer. Under inert atmosphere (nitrogen, as carrier gas) with flow of 20 cm^3 min^{-1}, thermogravimetric analysis was accomplished using Shimadzu TGA-50H thermal analyzer with 10 °Celsius/min heating rate from 30 to 400 °C. Mass spectra (in m/z) were determined on waters Q-tof Micro YA263 mass spectrometer for the current compounds. pH was determined by a Metrohm 695 pH/ion meter to ±0.005 units with control of temperature by a HAAKE model F3-k as an ultrathermostat bath. The temperature of the melting point, in Celsius, was evaluated by a Thermo Scientific 9100 apparatus.

2.2 | Synthesis and characterization

2.2.1 | Synthesis of 1,2-bis[2-(2-Hydroxyphenyl)methylene] hydrazide (H_2L1) and 1,2-bis[2-(5-sodium sulfonate-2-hydroxyphenyl)methylene] hydrazide (H_2L2)

H_2L1 and H_2L2 were prepared according to the previously published method with little modifications.[2,29] Briefly, an aqueous solution of oxalyldihydrazide (5.0 mmol, 0.59 g dissolved in 20 ml water) was mixed with an aqueous solution of appropriate salicylaldehyde (10.0 mmol, 1.2 ml in 30 ml methanol) or salicylaldehyde derivative (*e.g.* 5-sodium sulfonate, 10.0 mmol, 2.2 g in 30 ml water). The resulted mixture was heated under reflux at 100 °C for 2 hr and the completion of the dihydrazone formation was detected by TLC. Methanol–water mixture was slowly removed under reduced pressure and the remaining slurry was washed by ethanol and purified by recrystallization from ethanol/water (1: 1) ratios.

1,2-bis[2-(2-Hydroxyphenyl)methylene]hydrazide (H_2L1)

^{1}H NMR (DMSO-d_6, 400.1 MHz) δ 6.93 (t, ^3J = 8.0 Hz, 4 H), 7.43 (t, ^3J = 8.1 Hz, 2 H), 7.56 (d, ^3J = 8.0 Hz, 1 H), 8.82 (s, 2 H), 11.00 (s, NH, 2 H) and 12.61 ppm (s br, 1 H, CH=N). ^{13}C NMR (DMSO-d_6, 100.6 MHz, dept-135): δ 116.69 (CH), 119.83 (CH), 126.86 (CH), 129.74 (CH), 131.53 (C_q), 47.07 (C_q), 156.72 (C_q) and 163.41 ppm (CH=N) (Figures S1 and S2).

IR spectra (KBr tablets); $\bar{\nu}$ = 3347 (O—$H_{phenolic}$), 3272 (N—H), 1719 (C=O), 1611 (C=N), 1584 (NH—CO), 1329 (C—O), and 1039 cm^{-1} (C—N).

1,2-bis[2-(5-sodium sulfonate-2-hydroxyphenyl) methylene]hydrazide (H_2L2)

^{1}H NMR (DMSO-d_6, 400.1 MHz): δ 6.87 (d, ^3J = 8.0 Hz, 2 H), 7.54 (dd, ^3J = 7.2 and 8.1 Hz, 2 H), 7.83 (d, ^3J = 2.2 Hz, 2 H), 8.82 (s br, 2 H, CH=N) and 11.00 ppm (s br, 2 H, —NH). ^{13}C NMR (DMSO-d_6, 100.6 MHz, dept-135): δ 116.01 (CH), 118.09 (C_q), 126.64 (CH), 129.92 (CH), 140.53 (C_q), 150.76 (C_q), 156.36 (C_q) and 157.95 ppm (CH=N) (Figures S3 and S4).

IR spectra (KBr tablets); $\bar{\nu}$ = 3328 (O—$H_{phenolic}$), 3186 (N—H), 3061 (C—$H_{aromatic}$), 1674 (C=O), 1611 (C=N), 1564 (NH—CO), 1012 (C—N), 1415 (S=O) and 1142 cm^{-1} (S—O). The yield was 4.83 g (91%).

2.2.2 | Synthesis of cis-bis-dioxomolybdenum (bis[2-(2-oxyphenyl) methylene]hydrazone) complex (MoO_2L1)

A solution of *cis*-$MoO_2(acac)_2$ (10.0 mmol, 3.26 g in 50 ml of water) and H_2L1 (5.0 mmol, 1.63 g in 50 ml methanol) were mixed together in a two-neck round bottom flask. The obtained mixture was heated under reflux for 4 hr. The solvent was slowly removed by evacuation. The remaining residue was washed by ethanol and purified by recrystallization from ethanol. The yield was 71%.

^{1}H NMR (DMSO-d_6, 400.1 MHz): δ 3.59 (s, 6 H, —CH_3, methanol), 6.95–7.01 (m, 4 H), 7.41 (dd, ^3J = 7.0 and 8.0 Hz, 2 H), 7.71 (d, ^3J = 7.0 Hz, 2 H) and 9.01 ppm (s br, 2 H, CH=N). ^{13}C NMR (DMSO-d_6, 100.6 MHz, dept-135): δ 57.71 (CH, —CH_3, methanol), 115.17 (CH), 118.95 (C_q), 125.95 (CH), 126.59 (CH), 141.92 (CH), 149.57 (C_q), 156.97 (C_q) and 166.12 ppm (CH) (Figures S5 and S6).

IR spectra (KBr tablets); $\bar{\nu}$ = 3496 (O—$H_{methanol}$), 3029 (C—$H_{aromatic}$), 1643 and 1558 (C=N), 1273 (C—O), 1032 (C—N), 910 (Mo—O) and 531 cm^{-1} (Mo—N).

2.2.3 | Synthesis of cis-bis-dioxomolybdenum bis[{2-(5-sodium sulfonate-2-oxyphenyl)methylene} hydrazone] complex (MoO_2L2)

A solution of *cis*-$MoO_2(acac)_2$ (10.0 mmol, 3.26 g in 60 ml of water) and H_2L1 (5.0 mmol, 2.56 g in 40 ml water) were mixed together in a two-neck round bottom flask. The mixture solution was heated under reflux for 4 hr. After that, the reaction mixture was cooled down and then the solvent was slowly evacuated. The remaining residue was washed by water and purified by recrystallization from ethanol/water (1:1) ratios. The yield was 68%.

^{1}H NMR (D_2O, 400.1 MHz): δ 3.71 (s, 4 H, H_2O), 7.04 (dd, ^3J = 8.1 Hz, 2 H), 7.88 (dd, ^3J = 8.7 and ^4J = 2.2 Hz, 2 H), 8.07 (d, ^4J = 2.2 Hz, 2 H) and 9.92 ppm (s br, 2 H, CH=N). ^{13}C NMR (D_2O, 100.6 MHz, dept-135): δ 117.99 (CH), 120.39 (C_q), 130.93 (CH), 133.90 (CH), 135.75 (C_q), 150.30 (C_q), 162.80 (C_q) and 186.88 ppm (—CH=N—) (Figures S7 and S8).

IR spectra (KBr tablets); $\bar{\nu}$ = 3400 and $1600_{overlaped}$ (O—H_{water}), 3047 (C—$H_{aromatic}$), $1600_{overlaped}$ (C=N), 1231 (C—O), 1011 (C—N), 1339 (S=O), 1124 (S—O), 901 (Mo—O) and 558 cm^{-1} (Mo—N).

2.3 | Molecular structural modeling (DFT)

Density Functional Theory (DFT) calculations were progressed in order to investigate the equilibrium geometry of the free ligands (H_2L1 and H_2L2) and their di-Schiff base complexes (MoO_2L1 and MoO_2L2) using Gaussian 09 program at the B3LYP/LANL2DZ level.[44] Their molecular geometrical structures were optimized within B3LYP and 6-31 g(d,p) for C, H, O, Mo, N, Na and S atoms in the gas phase.

2.4 | Catalytic procedures

Catalytic (ep)oxidation of 1,2-cyclooctene, benzyl alcohol and thiophene (1.0 mmol) was preceded by adding either 3.0 mmol of H_2O_2 (30% in water) or 1.7 mmol of *tert*-butyl hydroperoxides (*t*BuOOH, 70% in water), as an external oxidizing agent. The catalytic protocol was catalyzed by involving catalytic amounts of *cis*-MoO_2-chelates (0.02 mmol) in 10 mL of H_2O at 85 °C in an oil bath with magnetic stirring for the optimized time in under air atmosphere. The catalytic protocols were followed and controlled to assign the best required time for the highest percentage amount of the chemoselective product by taking ~ 1.0 ml samples of the catalytic reaction mixture at the exact interval time. The taking samples were treated with ~ 0.02 g of sodium persulfate to destroy the excess unreacted oxidant, *i.e.* H_2O_2 or *t*BuOOH. The obtained slurry was filtered. The chemoselective products were extracted from water by adding diethyl ether (2 ml). The organic layer containing the chemoselective products was submitted for measuring the amount percentages by injection of a 1 μL to the GC.

Shimadzu Gas Chromatography-mass spectrometer of QP2010 SE model equipped by Rxi-5 Sil MS capillary column (30 m length × 0.25 mm ID × 025 um film thickness) was used to analyze the injected product sample solutions. Detection of the product samples was carried out in GC at 250 °C of the injection temperature and at 40 °C of the initial oven temperature, which held at the given temperature for 1 min. Then the oven temperature was enhanced gradually with a rate of 10 °C min^{-1} up to 200 °C. The operated inlet was in the mode of the spitless. The mass spectra transfer line was held at 200 °C. Helium gas, as an inert GC-carrier gas, which pure with 99.999%, was applied with 1 mL min^{-1} of flow rate. Applying LabSolution software was necessary to deduce

the yield percentages of the chemoselective product. Define of resulted chromatogram peaks was realized by comparing to those resulted MS of the reported compounds with NIST mass spectra stored library.

2.5 | Molecular docking

Dell Precision™ T3600 Workstation equipped with Intel Xeon E5–1660 3.3GHz, 16GB 1600MHz DDR3, ECC RDIMM 1 TB (7200RPM), 1GB NVIDIA Quadro 2000, Windows 7 Professional (64 Bit), was machined to study the molecular docking of H_2L1, H_2L2, MoO_2L1 and MoO_2L2 using software MOE (Molecular Operating Environment) package version 2019.0101.

X-ray analysis of a 1BNA dodecameric d (CGCG AATTCGCG)2 crystal structure within 3′-5′direction (ctDNA code: 1BNA) was used for the examination the docking with 1.9 Å resolution. The introducing of the molecular structure of ctDNA with its hydrogen atoms could be calculated into MOE of the optimization of energy and the resulted geometrical model of the structure was proposed for the systematic confirmation research within a gradient of RMS of 0.01 kcal mol^{-1} with overlooking of parameters in the involved Site Finder device in MOE. Using ChemBioDraw Ultra 12.0, all studied current compounds were drawn for applying in the MOE. Then, the draw structure of H_2L1, H_2L2, MoO_2L1, and MoO_2L2 were concerned for the theoretical calculation of the molecular docking following three items: (1) involving of hydrogen atoms in the drawing of the molecular structure of all current compounds; (2) using the conformational search for them; (3) within the MMFF94 force field, the energy decreases with the optimal conformers.[45] Reducing of the energy along with the steepest algorithm was examined, with the trial of the conjugate gradient method till an RMS gradient reach to be 0.00001 kcal mol^{-1} $Å^{-1}$. Moreover, a database of H_2L1, H_2L2, MoO_2L1 or MoO_2L2 was obtained for more molecular docking studies. Moreover, in MOE 2016.08, the standard molecular docking was tested. The γ triangle position, which could derive poses by random superposition of H_2L1 and H_2L2 atoms triplets γ sphere dummies in the target site was used to determine the poses. The London dG scoring function exposed the ligand-free binding energy from the specified pose. The optimal docked molecules poses were assigned by more than 50 cycles of theoretical calculations. The achieved molecular dock file was produced with H_2L1, H_2L2, MoO_2L1 and MoO_2L2 different poses with a reconsideration of the final score function (*S*). The final score, *S*, was not set as any. Investigation of the various poses, the browser of the resulted database was selected for the optimization.

2.6 | DNA binding studies

2.6.1 | ctDNA interaction (UV–visible spectroscopy)

Electronic absorption measurements were performed at pH = 7.23 using *tris*-(hydroxymethyl)aminomethane-HCl buffer solution at the wavelength range 200–800 nm and at 25 °C. A UV-absorbance ratio of ctDNA was recorded at 260 and 280 nm, A260/A280, which in turn was higher than 1.8, indicating that there is no contaminated protein in the tested ctDNA. The background absorbance of ctDNA was eliminated by adding equal amounts of ctDNA to the MoO_2-complexes and the reference solutions.[8,9] Concentrated stock solution (1.0×10^{-3} M) of the free ligands (H_2L1 and H_2L2) and the MoO_2-complexes (MoO_2L1 and MoO_2L2) were also prepared in Tris–HCl and NaCl solution (10: 1). Titration experiments were performed by varying ctDNA concentration with maintaining the *cis*-MoO_2-complexes concentrations' constant. The binding constant, expressed as K_b for the interaction of the complex with ctDNA [DNA], could be derived from absorption spectral titration data by plotting $[DNA]/(\varepsilon_a - \varepsilon_b)$ versus the various concentrations of ctDNA, as [DNA], using Equation (1)[8,9,23,24]:

$$\frac{[DNA]}{\varepsilon_a - \varepsilon_f} = \frac{[DNA]}{\varepsilon_b - \varepsilon_f} + \frac{1}{[K_b(\varepsilon_b - \varepsilon_f)]} \quad (1)$$

where, [DNA] in mmoles is the ctDNA concentrations in the nitrogenous base pairs. All values of ε_f, ε_a and ε_b are presented as the extinction coefficients of free ctDNA with the MoO_2-complexes (MoO_2L1 or MoO_2L2), respectively. The calibration curves for the free MoO_2L1 and MoO_2L2 complexes, A_{abs}/[complex] could be calculated, as well as, the calibration curve for the free ctDNA, was also determined by A_{abs}/[DNA]. The values ε_f and ε_a were derived for both studied Mo-complexes and ctDNA, respectively. K_b was derived from the plot slope and the plot intercept ratio of the above plotting. The standard Gibb's free energy, $\Delta G_b^{\neq}$, for the interacted ctDNA with MoO_2L1 or MoO_2L2, was obtained from Equation (2)[8]:

$$\Delta G_b^{\neq} = -RTlnK_b \quad (2)$$

The category and magnitude of the chromism for each Mo-complex were appreciated according to Equation (3):

$$\text{Chromism}, \% = \frac{A_{free} - A_{bonding}}{A_{free}} \quad (3)$$

where A_{free} and $A_{bonding}$ are the significant absorbance values of the MoO_2L1 and MoO_2L2 solution without and with various concentrations of ctDNA at their characteristic maximum absorption wavelength.

2.6.2 | Hydrodynamic measurements

Hydrodynamic viscosity measurements were performed in order to give more evidence about the binding mode between the reacted ctDNA and the current *bis*-dioxomolybdenum complexes.[4,9] The hydrodynamic measurements were performed using Oswald microviscometer at 25 °C. Briefly, different concentrations (5.0–50.0 μM) of MoO_2-complexes (MoO_2L1 or MoO_2L2) were added to a defined concentration of ctDNA (250 mM). The resultant mixture was kept at 37 °C for 10 min with detection of the flow time rate by a digital stopwatch. Each run was repeated three times and the calculated average flow time was subsequently determined. From Equation (4), the particular viscosities η° and η were determined in the absence and presences of different concentrations of MoO_2L1 or MoO_2L2 to ctDNA, respectively[8,9,23,24]:

$$\eta = \frac{t - t^{o}}{t^{o}} \tag{4}$$

where, t is the fluid time of the reacted MoO_2L1 or MoO_2L2 with ctDNA and t° is the buffer fluid time in the absence of the reacted MoO_2-complexes (seconds). The ratios of the measured viscosities, η/η°, were plagiaristic from the plot of the viscosity with the reciprocal of *R*. Hence, *R* could be defined from Equation (5):

$$R = \frac{[DNA]}{[Compound]} \tag{5}$$

The [DNA] refers to the concentration of ctDNA (250 mM), whereas, [compound] refers to the various concentrations (5.0–50.0 μM) of MoO_2L1 or MoO_2L2.

2.7 | Anticancer potential

The anticancer activities of the *cis*-MoO_2-complexes (MoO_2L1 and MoO_2L2) and their free *bis*-Schiff base ligands (H_2L1 and H_2L2) were tested using MTT and Sulfo-Rhodamine-B stain (SRB) assays against colon carcinoma (HCT-116), breast adenocarcinoma (MCF-7) and human liver carcinoma (HepG2) cell lines purchased from the National Institute of Cancer in Cairo (Egypt) and in the Department of Cancer Biology, Pharmacology Department, Cairo University (Egypt). Cells were grown in a humidified atmosphere containing 15% (*v*/v) CO_2 in air. The medium used was Dulbecco's modified Eagle's supplemented with 100 mg ml^{-1} streptomycin sulfate, 60 mg ml^{-1} penicillin G and 10% (v/v) calf serum.

3-(4,5-dimethylthiazol-2-yl)2,5-diphenyltetrazolium bromide (MTT) was employed to estimate the cell viability of the living cells, which formed purple-colored formazan crystals.[46,47] Stock solutions of the tested compounds (10 and 5 mM) were prepared in sterilized DMSO. Briefly, in 96-well microplates, 50,000 cells mL^{-1} (120 μL cell suspension) were seeded and cultured for 48 hr at 37 °C and 10% CO_2 for optimal adherence. Then the medium was removed and 200 μL of diluted concentration series of the tested *cis*-MoO_2-compounds in a fresh medium were added with further incubation of the cells for more 48 hr. MTT solution (75.0 μL) in phosphate-buffered saline (PBS) was added and kept for two hr at 37 °C. The formed formazan crystals (precipitate) were centrifuged and the supernatant was removed. The purple formazan crystals were carefully washed three times with 100 μL of PBS and then solubilized in 100 μL DMSO. ELISA plate reader was used to estimate the intensity of the produced color at 590 nm. Experiments were repeated twice and the IC_{50} values are defined when the various concentrations of current compounds produce 50% of the absorbance of untreated cells. 5-Fluorouracil was used as a positive control.

The sulfo-Rhodamine-B stain assay was used to evaluate the cytotoxicity of the prepared agents employing the known reported method Ayuso, et al.[48] This experiment was also performed at the National Cancer Institute, Cairo University. Briefly, cells were cultured in 96-multiwell microtiter plate (10^4 cells/well) for twenty-four hours for optimal adherence. Test compounds were solubilized in DMSO and diluted with saline buffer to the desired concentration. Cells were then treated with serial concentrations of the test compounds and incubated for 48 hr at 37 °C and in an atmosphere of 5% CO_2. After routine fixation and washing, cells were stained with 0.4% (wt vol^{-1}) SRB for a half-hour. Cells were then washed 4X with 1% acetic acid to get rid of excess dye and recovered again via Tris-EDTA buffer. ELISA reader was accomplished to adjust the intensity values of color an enzyme-linked immunosorbent assay. This experiment was performed at least three times. The survival curve of tumor cells was estimated by plotting drug concentration versus the surviving fraction.

2.8 | Antioxidant activity

2.8.1 | DPPH assay

Free radical scavenging potential of MoO_2L1 and MoO_2L2 was studied by the DPPH radical scavenging

assay by following the disappearance of the DPPH solution purple color in methanol to pale yellow color. Briefly, 2.40 ml of DPPH in methanol (0.1 mM) was poured into a 100 μM methanolic solution of MoO_2L1 and to an aqueous solution of MoO_2L2. The obtained mixture was vortexed in a dark place at room temperature for 0.5 hr. The molar absorptivity of the final obtained mixed solution was determined at 517 nm calorimetrically. Vitamin C (ascorbic acid) was involved as a positive control.[49] The negative control (only methanol) and a blank sample (no DPPH) were also performed for comparison. The DPPH % of radical scavenging capacity was estimated by applying Equation (6):

$$\text{Radical scavenging}\% = \left(\frac{A_o - A_s}{A_o}\right) \times 100 \qquad (6)$$

where, A_o is the control activity and A_s is the sample activity.

2.8.2 | SOD assay

The activity of superoxide dismutase (SOD) was explored in the absence and presence of MoO_2L1 and MoO_2L2, spectrophotometrically with SOD kit.[50] The ability of the enzyme to inhibit the reactivity of phenazine methosulphate-mediated reduction was investigated by nitro blue tetrazolium dye.[51] The remarkable shift in the maximum absorption bands (560 nm) for more than 5 min and then the intimating percentages were evaluated.

2.9 | Antimicrobial activity

The antibacterial potential of the studied ligands (H_2L1 and H_2L2) and their corresponding Mo-chelates (MoO_2L1 and MoO_2L2) were examined using two Gram-negative (*Serratia Marcescence* and *Escherichia coli)* and one Gram-positive (*Staphylococcus aureus*) bacterial strains. The fungal strains *Candida albicans*, *Aspergillus flavus,* and *Trichophyton rubrum* were also used to assess the compounds' antifungal activity.

The antimicrobial potential was predestined using the known agar well diffusion method employing 100 μL of fungal/bacterial suspension (1.0×10^4 pores ml^{-1} of fungi and 1.0×10^8 CFU ml^{-1} of the bacterial strains) spread on potato dextrose agar, and nutrient agar medium, respectively.[51] 6 mm diameter paper discs soaked with 20 μM of the compounds were put on the agar plates and hold at 30 °C for 24 hr, the antimicrobial activities were estimated by measuring the inhibition zone and compared with the standard antibacterial drug ofloxacin and the antifungal fluconazole drug positive controls. The % activity index was computed following Equation (7):

$$\%\text{activity index} = \frac{(\text{inhibition zone of the test compounds}}{\text{inhibition zone of the standard drug}} \times 100 \qquad (7)$$

Moreover, the minimum inhibitory concentrations (MIC) in mM of the tested compounds were determined by the microdilution method following the reported method.[51] The MIC was calculated after 18–20 hr and defined as the lowest concentration of compound giving complete inhibition of growth.

3 | RESULTS AND DISCUSSION

3.1 | Synthesis and structure evaluations

Salicylaldehyde is commonly used for the preparation of a wide range of Schiff bases for various proposes.[52] The use of salicylidene hydrazone *bis*-analogs is however less common in coordination chemistry.[53] It was therefore aimed to base our design criteria of *cis-bis*-dioxomolybdenum complexes on the use of *bis*-salicylidenedihydrazone ligands. Two bidentate *bis*-Schiff base ligands (H_2L1 and H_2L2) derived from salicylaldehyde and oxalyldihydrazide[25] were synthesized following the reported literature methods.[54] It is worth noting that, H_2L2 ligand bearing the hydrophilic sodium sulfonate groups was used here as a water-soluble analog. The synthesis of H_2L1 and H_2L2 ligands and their related MoO_2-complexes is outlined in Scheme 1. The structures of H_2L1 and H_2L2 ligands were elucidated by ^{1}H- and ^{13}C-NMR, IR, mass and ultraviolet–visible spectra, as well as elemental analyses (EA) and conductivity measurements.

3.2 | The *cis-bis*-dioxomolybdenum complexes features

The *bis*-dioxomolybdenum complexes MoO_2L2 and MoO_2L2 were obtained *via* the reaction of *cis*-$MoO_2(acac)_2$ with H_2L1 and H_2L2 ligands in 2: 1 ratio with good yield percentages (74 and 69%), respectively. The solid phase of Mo-complexes is stable, which decompose at higher than 300 °C without melting (Table 1). *Bis*-dioxomolybdenum (II) ion coordinated to H_2L1 and H_2L2 to form homo-*bis*-dinuclear pincer chelates within 2: 1 equivalent of *cis*-$(MoO_2)^{2+}$: ligand, respectively. The tentative molecular structure of the *cis*-MoO_2-complexes

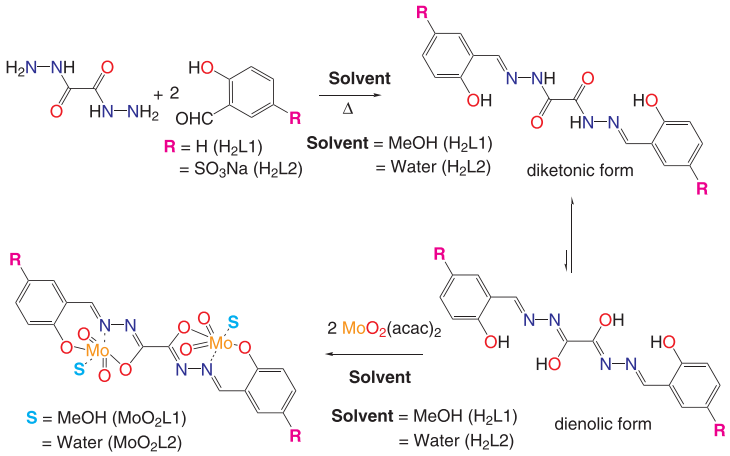

SCHEME 1 The preparation of H_2L1, H_2L2 and their *cis*-MoO_2-complexes (MoO_2L1 and MoO_2L2)

was in good agreement with other reported *cis*-MoO_2-complexes in the literature.[55] The stoichiometric molar ratios of $(MoO_2)^{2+}$-ions and H_2L1 or H_2L2 solutions were estimated by the common spectrophotometric continuous variation method (Figure S9).

The obtained continuous variation plots established that all MoO_2-complexes formed in one equivalent of ligand and two equivalents of *cis*-$(MoO_2)^{2+}$ ion. Alternative physico-chemical tools were applied to characterize and elucidate the molecular structures of MoO_2L1, and MoO_2L2 (Table 1). The resulted data of the elemental analyses of the *cis*-MoO_2-chelates, as listed in Table 1, were in good harmony with those theoretical data for the suggested molecular formulae. The standard universal buffers, which controlled the pH range of the ligands and their MoO_2-complexes stability, assigned from 2.3 to 10.1 (Figure 1).[25]

H_2L1 and MoO_2L1 are soluble in chloroform, dichloromethane and also in strong coordinating solvents such as dimethylsulfoxide (DMSO) and *N*,*N*′-dimethylformamide (DMF). On the other hand, H_2L2 and MoO_2L2 are completely soluble in water as well as DMSO and DMF. H_2L1, H_2L2, MoO_2L1, and MoO_2L2 showed spring solubility in most of the common organic high polar solvents, *e.g.* acetonitrile and methanol. The *p*-sodium sulfonate substituent in H_2L2 and MoO_2L2 is responsible for its solubility in water and this facilitated their conductivity features investigation in water. Three counter ions were included in the solution for each molecule of H_2L2 or MoO_2L2 since two of them are Na^+ ions and the third ion is the complex anion as disulfonate anion.[29]

3.2.1 | NMR spectra

Further details on the spectrum data and copies of ^{1}H- and ^{13}C-NMR spectra are assigned in the supplementary materials (Figures S1-S8). The characteristic singlet resonating signals of NH— protons at 11.00 and 8.82 ppm for both H_2L1 and H_2L2 were completely disappeared after complexation to *cis*-$(MoO_2)^{2+}$ ions. *Cis*-$(MoO_2)^{2+}$ ions forced the enolized form of H_2L1 or H_2L2 to coordinate with *cis*-$(MoO_2)^{2+}$ ions. The high remarkable shift of the boarded singlet signals of —CH=N—, Schiff base group, were assigned from 12.61 and 11.00 ppm H_2L1 and H_2L2 to 9.01 and 9.92 ppm in MoO_2L1 and MoO_2L2, respectively. The coordinating ability of the nitrogen lone pair of the Schiff base moiety to *cis*-$(MoO_2)^{2+}$ ions could be responsible for that strong shift. In ^{13}C-NMR spectra, the downfield shift of the significant Schiff base group form 163.41 and 157.95 ppm in H_2L1 and H_2L2, respectively, to 166.12 and 186.88 ppm in MoO_2L1 and MoO_2L2, respectively, could be due to the coordination of the nitrogen lone pair of the Schiff base group to *cis*-$(MoO_2)^{2+}$ ions. Moreover, the appearance of strong downfield shift signals at 156.97 and 162.80 ppm after complexation in MoO_2L1 and MoO_2L2, respectively, could be resulted from the presence of dienolized tautomer. *Cis*-$(MoO_2)^{2+}$ ion coordinated to the dienolized tautomer of H_2L1 or H_2L2 (Scheme 1).[29]

3.2.2 | Ultraviolet–visible spectroscopy

The characteristic electronic transitions of H_2L1, H_2L2, MoO_2L1 and MoO_2L2 were assigned at the maximum absorption wavelength (λ_{max}) and shown in Table 1 and in Figure 2. In the UV-area, H_2L1 and H_2L2 exhibited two characteristic high-energy bands of $\pi \rightarrow \pi^*$ transition at 248 and 249 nm and $n \rightarrow \pi^*$ transition at 326 and 291 nm, respectively. Moreover, an observable absorption band at 393 and 353 nm for H_2L1 and H_2L2, respectively, due to the electronic transition of the ligand charge transfer.[5,19] The binding of the coordinated ligands to *cis*-$(MoO_2)^{2+}$ ions caused an observable shift of the above

TABLE 1 CHN analyses, melting point, electronic spectral transitions of H_2L1 and MoO_2L1 in methanol, and H_2L2 and MoO_2L2 in water at [compound] = 1.0×10^{-5} mol dm^{-3} and 25 °C. Molar conductivities, Λ_m, of [compound] = 1.0×10^{-3} in mol dm^{-3} in H_2O, DMF or DMSO at 25 °C

Comp.	MW (g mol^{-1})	Color	CHN analysis found %, (calc. %)				m.p. (°C)	UV–Vis. spectra			Λ_m ($\Omega^{-1}.cm^2.mol^{-1}$)		
			C	H	N			λ_{max} (nm)	ε (mol^{-1} cm^{-1})	Assign.	H_2O	DMF	DMSO
H_2L1	326.31	Pale yellow	59.18 (58.89)	4.00 (4.32)	16.87 (17.17)		207	393 326 248	5134 8041 10457	L-CT n → π^* $\pi \rightarrow \pi^*$	--	--	--
MoO_2L1	642.28	Orange	33.21 (33.66)	3.01 (2.82)	9.02 (8.72)		277	500 359 321 300 246	4893 7399 7420 7495 11301	d → d ML-CT n → π^* n → π^* $\pi \rightarrow \pi^*$	--	--	--
H_2L2	530.39	Yellow	36.15 (36.23)	2.33 (2.28)	10.19 (10.56)		264	353 291 249	5719 6182 15002	L-CT n → π^* $\pi \rightarrow \pi^*$	363	232	209
MoO_2L2	818.30	Reddish orange	23.22 (23.48)	1.21 (1.48)	7.13 (6.85)		> 300	475 346 318 245	5010 5748 7080 13898	d → d ML-CT n → π^* $\pi \rightarrow \pi^*$	401	218	188

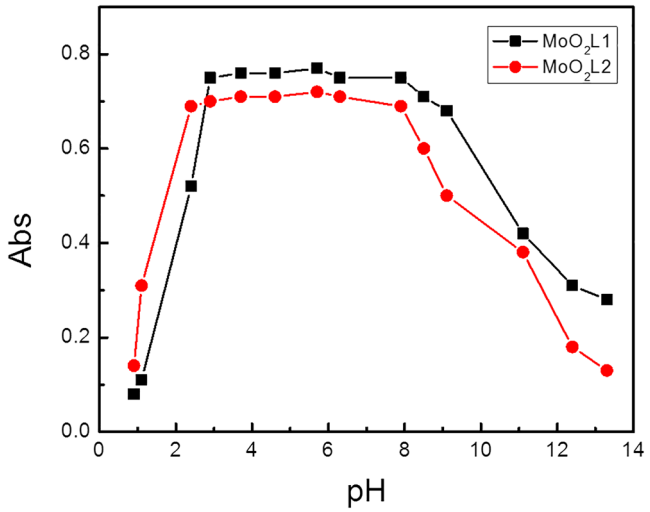

FIGURE 1 pH effect on the stability of a methanolic solution of MoO_2L1 and an aqueous solution of MoO_2L2

characteristic bands. Both π → π* and of *n* → π* electronic transitions were little shifted to lower energy values (246, 300 and 315 nm, respectively for MoO_2L1 and 245 and 318 nm for MoO_2L2, respectively). Particularly, the ligand-CT band was also shifted but with a remarkable value to the lower energy area at 359 and 346 nm, for MoO_2L1 and MoO_2L1, respectively. The most detected characteristic broad-band at 500 and 475 nm for MoO_2L1 and MoO_2L1, respectively, was resulted from the complexation and from the *d* → *d* electronic transition of *cis*-$(MoO_2)^{2+}$ ion in its complexes.

3.2.3 | IR spectra

IR spectra of H_2L1, H_2L2, MoO_2L1 and MoO_2L2 are documented in the supplementary materials (Figures S10-S13). From the displayed absorption signals of IR spectra, the diagnostic characteristic absorption signals of the phenolic OH-dihydroxyl group (3347 and 3328 cm^{-1}) and NH-diimino group (3272 and 3186 cm^{-1}) in H_2L1 and H_2L2, respectively, were completely disappeared due to the bonding of the deprotonated phenolic-hydroxy group and the dienolized form of H_2L1 and H_2L2 in their MoO_2-complexes. The stretching vibrational bands of >C=O bonds were also disappeared in H_2L1 and H_2L2 (1719 and 1674 cm^{-1}, respectively) after complexation with appearing of new vibrational bands of —C=N— group at 1643 and 1600 cm^{-1}, respectively, this could prove that the dienolized tautomer was the coordinated form to *cis*-$(MoO_2)^{2+}$ ions, as reported previously.[29] Furthermore, the classified azo-methine group band (1611 cm^{-1} for H_2L1 and H_2L2) was remarkable shifted to 1558 cm^{-1}, respectively. This behavior could result from the

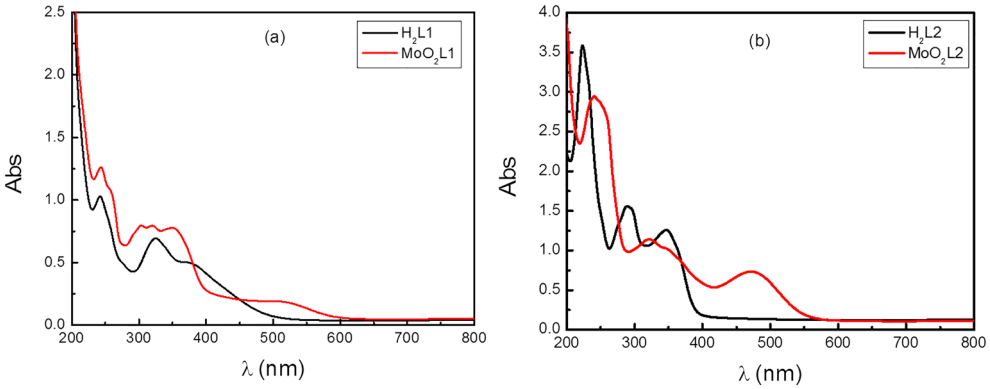

FIGURE 2 The electronic spectral scans of H_2L1 and MoO2L1 in methanol (a), H_2L2; and MoO_2L2 in water (b)

bonding of nitrogen lone pair of —C=N— group to *cis*-$(MoO_2)^{2+}$ ion.[4,5] The labile coordinated solvent molecules, *i.e.* methanol in MoO_2L1 and water in MoO_2L2, could be also confirmed by the presence of new stretching rotational bands at $\bar{\nu}$ = 3496 and 1599 cm^{-1} for the methanol molecules in MoO_2L1 and 3400 and 1600 cm^{-1} for the water molecules in MoO_2L2.[54] The *p*-sodium sulfonate group in H_2L2 had two distinguished stretching vibrational bands at 1142 and 1415 cm^{-1} corresponded to the S—O^- and S=O bonds, respectively, which have been little shifted to 1124 and 1339 cm^{-1} in MoO_2L2, respectively, due probably to the complexation to *cis*-MoO^{2+} ions.[54] Additionally, new characteristic absorption bands were detected at 910 and 901 cm^{-1} in MoO_2L1 and MoO_2L2, respectively, resulted from the formed M—O bonds. Also, other weak bands at 531 and 558 cm^{-1} were referred to the M—N bonding in MoO_2L1 and MoO_2L2, as reported elsewhere for Mo—O and Mo—N bonding.[25,29]

3.2.4 | Mass spectra

Mass spectroscopic results for H_2L1, H_2L2, MoO_2L1 and MoO_2L2 are recorded in supplementary materials (Figures S14-S17). The mass peaks that appeared at 327 m/z belong to H_2L1 and at 643, 648 and 649 m/z for [M + 1] for MoO_2L1, respectively. H_2L1 and MoO_2L1 showed peaks of [M + 1] at 531 m/z for H_2L1 and at 819, 820, 822, 824, 826 and 828 m/z for MoO_2L1. Other base peaks of [M - Na^+] exhibited at 485 m/z for H_2L2 and at 772 m/z for MoO_2L2. Moreover, base peaks of [M - SO_3Na^+] assigned at 362 m/z for H_2L2 and at 612 m/z for MoO_2L2.

3.2.5 | Thermogravimetric analyses

In order to obtain useful information about the thermal stability of the prepared metal chelates and to decide whether the methanol and water molecules are inside or outside the inner coordination sphere of the metal, thermal analysis was carried out.[56,57] The number of the labile coordinated solvent molecules, *i.e.* methanol in MoO_2L1 and MoO_2L2, respectively, were investigated by thermogravimetric analyses (TGA). TGA results are shown in supplementary materials Figure S18. The thermogram presents a notable decomposed sequential step in the range of 200 to 260 °C. The mass percentage loss was found to be $\Delta m_{exp.}$ = 10.5 and 5.0%, which approximately convenient with the predictable mass loss ($\Delta m_{cal.}$ = 9.9 and 4.4% for MoO_2L1 and MoO_2L2, respectively). The mass loses percentage referred to the two coordinated methanol molecules in MoO_2L1. Similarly, the loss percentage of the coordinated water molecules in MoO_2L2 referred to the two water molecules' loss in that temperature range.[29]

3.3 | DFT results

The optimized geometrical structure of H_2L1, H_2L2, MoO_2L1 and MoO_2L2 is presented in Figure 3 with the lowest energy configurations resulted from DFT studies. The natural charges of the current compounds were obtained from Natural Bond Orbital Analysis (NBO). For H_2L1, NBO showed that the more negative active sites were on O1 (−0.554), O2 (−0.633), O3 (−0.729), O4 (−0.732), N1 (−0.479), N2 (−0.462), N3 (−0.255) and N4 (−0.238). From NBO analyses of MoO_2L1, Mo atom had six-coordinated bonds in an octahedral geometry. Mo1 atom coordinated to O2, N4, O3 and O7 of H_2L1, which were almost in one plane with little deviation by 3.243°. Mo2 atom was coordinated to N3, O4, O6 and O10, which were, similarly, in one plane and deviated by 5.568°. The bond angles in the octahedral around Mo1 atom were ranging from 72.94° to 103.7° and the bond angles in the octahedral around Mo2 atom were ranging from 70.05° to 107.7°, as listed in Table S1 (Figure S19 in the supplementary materials). The distances between

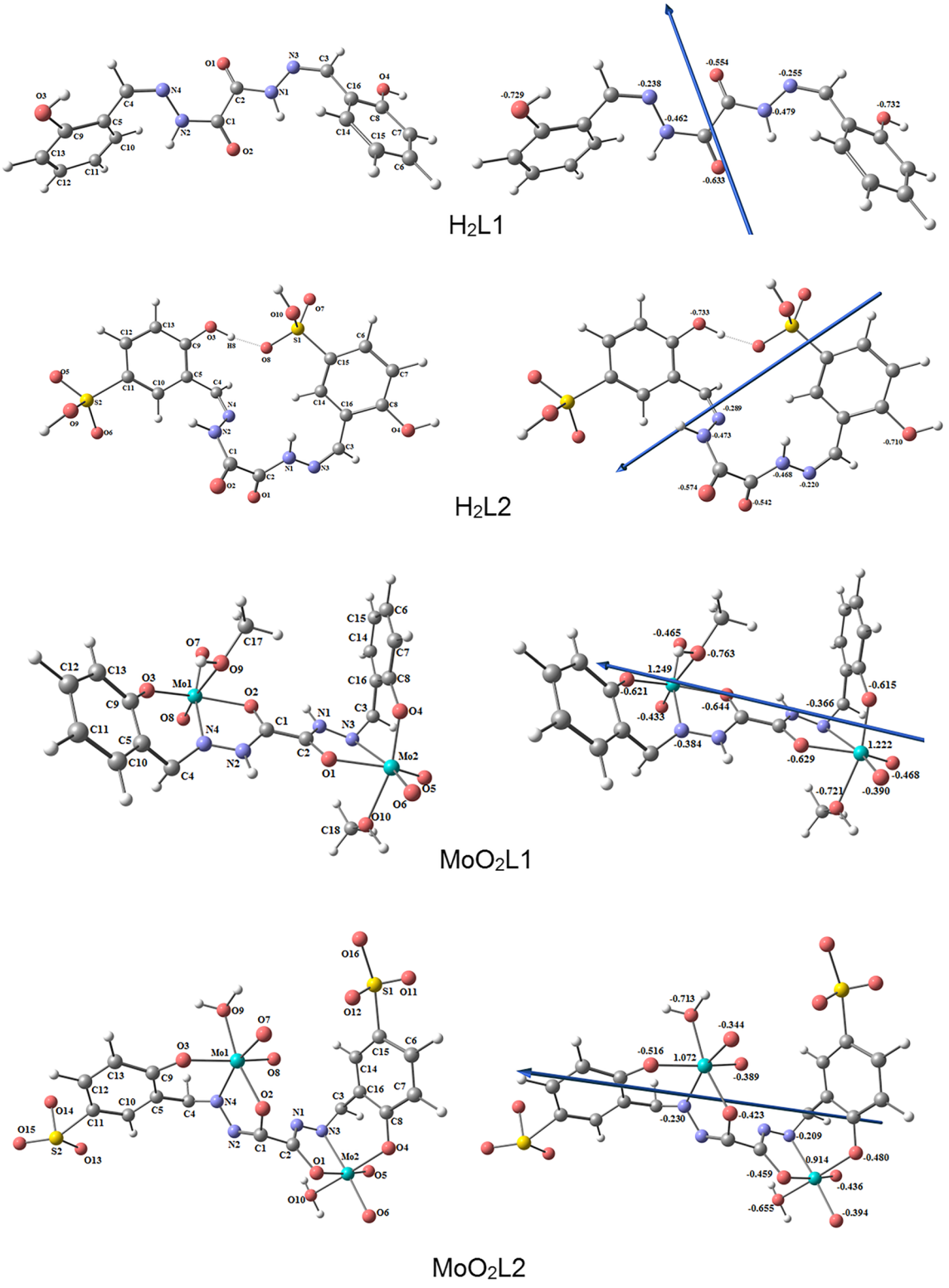

FIGURE 3 The optimized structure, the vector of the dipole moment, and the natural charges on active centers of H_2L1, H_2L2, MoO_2L1, MoO_2L2 using B3LYP/LANL2DZ

donor atoms in H_2L1 were longer than those in MoO_2L1, due to their coordination to *cis*-$(MoO_2)^{2+}$ ion, Table 2. Furthermore, the natural charges, which derived from NBO-analyses, were found on Mo1 (+1.244) and Mo2 (+1.180), as positive charges, and also found on O1 (−0.585), O2 (−0.600), O3 (−0.700), O4 (−0.620), O5 (−0.439), O6 (−0.376), O7 (−0.445), O8 (−0.494), O9 (−0.725), O10 (−0.708), N3 (−0.378) and N4 (−0.391), as

TABLE 2 Comparison between distances of coordinated atoms in H_2L1, H_2L2, MoO_2L1 and MoO_2L1

	Bond length (Å)			Bond length (Å)	
Type of bond	**H_2L1**	**MoO_2L1**	**Type of bond**	**H_2L1**	**MoO_2L1**
N4⋯⋯ O2	3.556	2.545	N3⋯⋯ O1	2.824	2.64
N4⋯⋯ O3	4.027	2.666	N3⋯⋯ O4	3.944	2.766
O2⋯⋯ O3	6.754	3.884	O1⋯⋯ O4	6.683	2.906
	H_2L2	MoO_2L2		H_2L2	MoO_2L2
N4⋯⋯ O2	3.550	2.536	N3⋯⋯ O1	2.819	2.645
N4⋯⋯ O3	4.045	2.814	N3⋯⋯ O4	3.945	2.876
O2⋯⋯ O3	6. 889	3.256	O1⋯⋯ O4	6.745	2.897

negative charges, Figure 3. For H_2L2, the most negative active sites were found on O1 (−0.542), O2 (−0.574), O3 (−0.733), O4 (−0.710), N1 (−0.468), N2 (−0.473), N3 (−0.220) and N4 (−0.289).

In MoO_2L2 within an octahedral geometry, Mo1 atom had O2, N4, O9 and O7, which was almost in one plane with deviation by 6.003°. Atoms of O1, N3, O5 and O6 coordinated to Mo2 atom in MoO_2L2, which deviated from one plane by 0.583°. The bond angles in the octahedral around Mo1 atom were in the range from 75.14° to 116.5° and the bond angles in the octahedral around Mo2 atom were in the range from 80.93° to 94.28° (Table S2 and Figure S19 in the supplementary materials). The distances between donor atoms in H_2L2 were longer than those in MoO_2L2, which due to its coordination to $(MoO_2)^{2+}$ ions (Table 2). The natural distributed charges, which computed by NBO-analyses on the coordinated atoms, were recorded as Mo1 (+1.072), Mo2 (+0.914), O1 (−0.459), O2 (−0.423), O3 (−0.516), O4 (−0.480), O5 (−0.436), O6 (−0.394), O7 (−0.344), O8 (−0.389), O9

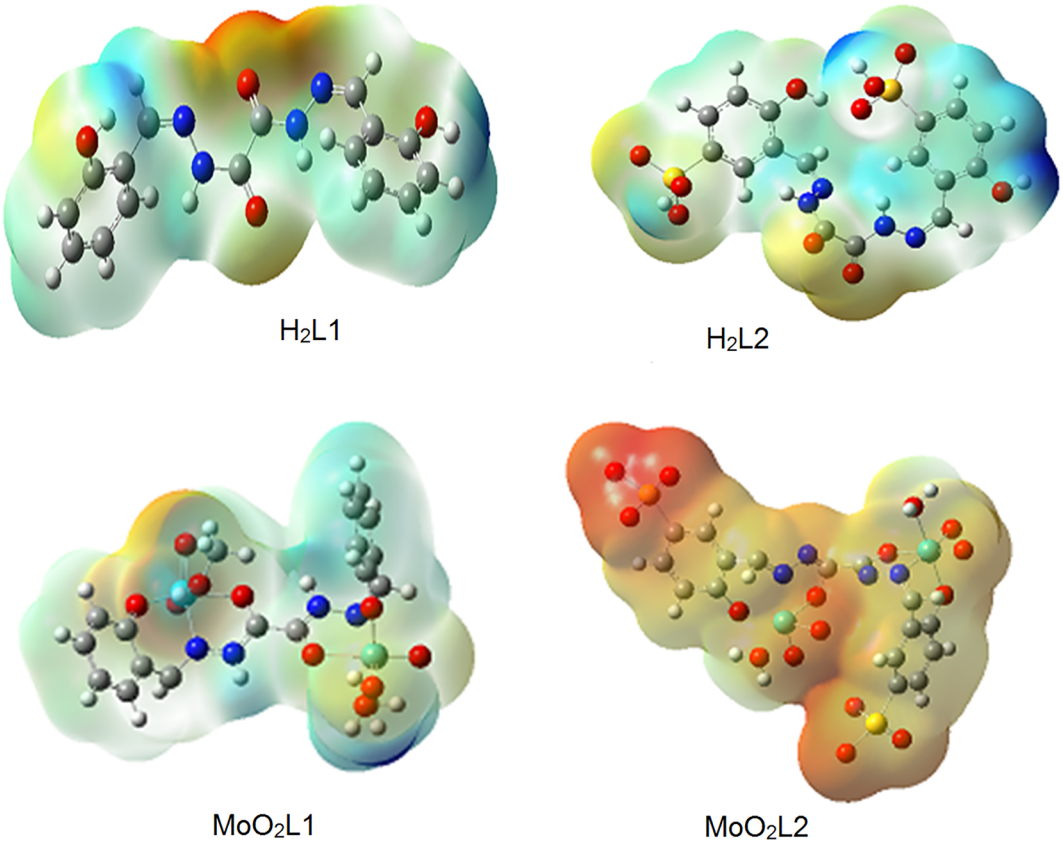

FIGURE 4 Molecular electrostatic potential (MEP) surface of H_2L1, H_2L2 and their complexes (MoO_2L1 and MoO_2L2) using B3LYP/LANL2DZ

(−0.713), O10 (−0.655), N3 (−0.209) and N4 (−0.230), Figure 3.

The MEP surface, which presented in Figure 4, shows the location of the positive (blue color) and negative (red color, *i.e.* bound loosely or excess electrons) charged electrostatic potential in the molecule. The total computational energy, the highest occupied molecular orbital (HOMO) energies, the lowest unoccupied molecular orbital (LUMO) energies and the dipole moment of H_2L1, H_2L2, MoO_2L1 and MoO_2L2 were calculated and listed in Table 3. The high stability of MoO_2L1 and MoO_2L2 compared to that of the coordinated ligands (H_2L1 and H_2L2) could be estimated by their more negative magnitudes of total energy than those of free ligands. Also, the energy gap (ΔE_g), which assigned by the difference in values between E_{LUMO} and E_{HOMO}, was smaller values for MoO_2L1 and MoO_2L2 than those for the free H_2L1 and H_2L2, respectively, due to chelation effect of ligand to metal ions, Table 3.[9] The low magnitude of ΔE_g for MoO_2L1 and MoO_2L2 compared to that of l H_2L1 and H_2L2 was probably due to the charge transfer interactions within the complex formation. Finally, all the theoretical results agreed with the experimental obtains for the Mo-complexes formation.

3.4 | Catalytic (ep)oxidation studies

A comparative catalytic study was performed between the less and high polar homo-dinuclear complex catalysts (MoO_2L1 and MoO_2L2), respectively, in the (ep)oxidation of 1,2-cyclooctene, benzyl alcohol and thiophene in water under sustainable reaction conditions. Due to the most applicability in the literature of the dioxo- and peroxomolybdenum Schiff base chelates as appreciated homogenous catalysts for (ep)oxidation protocols under alternative conditions,[32,58–60] both MoO_2L1 and MoO_2L2 were involved in various (ep)oxidation systems. The chemoselective products of 1,2-cyclooctene, benzyl alcohol and thiophene (ep)oxidation by H_2O_2 or *t*BuOOH catalyzed by MoO_2L1 or MoO_2L2 are 1,2-epoxy-cyclooctane, benzaldehyde and thiophene oxide.[28,61,62] The chemoselective yield percentages were detected by GC–MS. There are reported well-known side products of benzyl alcohol and thiophene oxidation which are benzoic acid and thiophene dioxide.[28,29] The catalytic potential of the less polar catalyst (MoO_2L1) and the high polar one (MoO_2L2) was investigated and measured by the yield amounts of the chemoselective product percentages, which determined and list in Tables 4 and 5. TONs and TOFs values were calculated also and recorded in Tables 4 and 5.

Both Mo (VI)-catalysts exhibited excellent catalytic reactivity for all oxidation processes with excellent conversion percentages (94–100%) using an aqueous H_2O_2 in water (Table 4), but unfortunately, only at high temperature (85 °C). The chemoselective amounts were alternatively in between excellent for 1,2-epoxy-cyclooctane percentages, good for benzaldehyde percentages and moderate for thiophene oxide percentages. The yields were 84, 78 and 40% at the optimized times (3, 1.5 and 2 hr) of 1,2-epoxy-cyclooctane, benzaldehyde and thiophene oxide, respectively, catalyzed by MoO_2L1 and oxidized by H_2O_2. The yield percentages with MoO_2L2 were remarkably more assigned in the same reaction conditions, which afforded 90, 88 and 47% at the optimal times (2, 1.5 and 2 hr) of 1,2-epoxy-cyclooctane, benzaldehyde and thiophene oxide, respectively, as observed in Figures S20-S22 in the supplementary materials (Table 4). As a consequence, MoO_2L2 seems to be more effective catalyst for all subjected catalytic processes than that MoO_2L1 with H_2O_2 (the most eco-friendly oxidant) in the aqueous media. Both catalysts took almost similar reaction time to reach the optimized amounts of the chemoselective product percentages due to their similar chemical structures. It is important to mention here that MoO_2L1 was very sparingly soluble in the reaction media, but after adding the oxidant, it was completely soluble.

The solubility and miscibility of the catalyst in the reaction media have observable influences on the

TABLE 3 Calculated energies of H_2L1, H_2L2 and their complexes (MoO_2L1 and MoO_2L2) at B3LYP/LANL2DZ

Compound	ΔE_g[a]	HOMO[b]	LUMO[c]	E_{gap}[d]	Dipole moment[e]
H_2L1	−1137.78	−6.3825	−2.2684	4.1141	4.114
MoO_2L1	−1804.14	−4.5677	−4.0238	0.5439	6.301
H_2L2	−1608.89	−7.2108	−3.5718	3.6390	15.020
MoO_2L2	−2193.50	−0.5606	−0.1298	0.4308	16.921

[a]E, the total energy (KCal mol^{-1}).
[b]HOMO, highest occupied molecular orbital (eV).
[c]LUMO, lowest unoccupied molecular orbital (eV).
[d]$E_g = E_{LUMO} - E_{HOMO}$ (eV).
[e]Dipole moment (Debye).

TABLE 4 Percentages of products yield of the catalytic (ep)oxidation of 1,2-cyclooctene, benzyl alcohol and thiophene using an aqueous H_2O_2 catalyzed by *cis*-MoO_2-complexes

Complex[a]	Time (hrs)	Reactant (%)	Product[b] (%)	Side product (%)	Conversion (%)	Selectivity (%)	TON[c]	TOF[d]
MoO_2L1	4	 (6%)	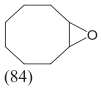 (84)	(10)[e]	94	89	89	22.3
		(6%)	(84)					
	2.5	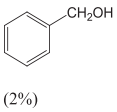 (2%)	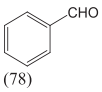 (78)	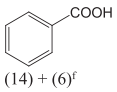 (14) + (6)[f]	98	79	79	31.6
		(2%)	(78)	(14) + (6)[e]				
	3.5	 (10%)	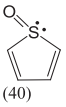 (40)	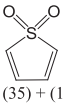 (35) + (15)[f]	90	44	44	12.6
		(10%)	(40)	(35) + (15)[e]				
MoO_2L2	2	 (1%)	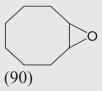 (90)	(9)[e]	99	91	91	45.5
		(1%)	(90)					
	1.5	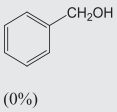 (0%)	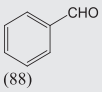 (88)	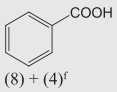 (8) + (4)[f]	100	88	88	58.7
		(0%)	(88)	(8) + (4)[e]				
	2	 (4%)	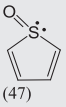 (47)	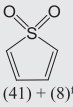 (41) + (8)[f]	96	49	49	24.5
		(4%)	(47)	(41) + (8)[e]				

[a]The (ep)oxidation reaction of the substrate (1.0 mmol) with H_2O_2 (3.00 mmol) catalyzed by MoO_2-complexes (0.01 mmol) in 10 mL water at 85 °C.
[b]The yield percentages derived from GC–MS results (%).
[c]TON (turnover number) = ratio of mmoles of the product (here oxide) to the mmoles of catalyst.
[d]TOF (turnover frequency) (TON/h) are shown in parentheses (mmoles (mmoles catalyst)$^{-1}$ h^{-1}).
[e]Other unknown side products are (%).

catalytic processes and could enhance the catalyst activity towards the (ep)oxidation reaction.[28,29] MoO_2L2 is highly soluble in water compared to MoO_2L1, which probably improved its catalytic potential in the (ep)oxidation of 1,2-cyclooctene, benzyl alcohol and thiophene more than that MoO_2L1, especially with the more polar oxidant, *e.g.* H_2O_2 in the aqueous media.[62]

Similarly, for the catalytic protocols with *t*BuOOH, the conversion percentages were little improved (94–100%), however, the chemoselectivity percentages were little reduced catalyzed with MoO_2L1 and MoO_2L2 in water (Table 5). With MoO_2L1, the yield percentages of 1,2-epoxy-cyclooctane, benzaldehyde and thiophene oxide were 88, 81 and 46% with the consumed ideal times (4, 2 and 2.5 hr), respectively, with little increase of the target product amount using *t*BuOOH compare to the above processes using aqueous H_2O_2.[63] Within MoO_2L2 as a homogeneous catalyst for all catalytic processes, both conversion and chemoselectivity were notably dropped and also the amount of the target products was lowered to be 85, 83 and 40% (4.5, 2 and 3 hr) of 1,2-epoxy-cyclooctane, benzaldehyde and thiophene oxide, respectively. The strong organic nature of the oxidant, *i.e.* *t*BuOOH, might be performed the catalytic potential

TABLE 5 Percentages of products yield of the catalytic (ep)oxidation of 1,2-cyclooctene, benzyl alcohol or thiophene using *t*BuOOH catalyzed by *cis*-MoO_2-complexes

Complex[a]	Time (hrs)	Reactant (%)	Product[b] (%)	Side product (%)	Conversion (%)	Selectivity (%)	TON[c]	TOF[d]
MoO_2L1	4	 (0%)	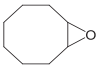 (88)	(12)[e]	100	88	88	22.0
		(0%)	(88)					
	2	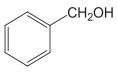 (0%)	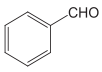 (81)	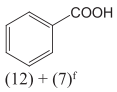 (12) + (7)[f]	100	81	81	40.5
		(0%)	(81)	(12) + (7)[e]				
	2.5	 (3%)	 (46)	 (39) + (12)[f]	97	47	47	18.8
		(3%)	(46)	(39) + (12)[e]				
MoO_2L2	4.5	 (2%)	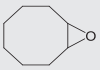 (85)	(13)[e]	98	87	87	19.3
		(2%)	(85)					
	2	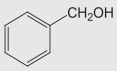 (0%)	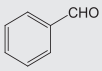 (83)	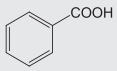 (11) + (6)[f]	100	83	83	41.5
		(0%)	(83)	(11) + (6)[e]				
	3	 (6%)	 (40)	 (36) + (18)[f]	94	42	42	14.0
		(6%)	(40)	(36) + (18)[e]				

[a]The (ep)oxidation reaction of the substrate (1.0 mmol) with *t*BuOOH (1.70 mmol) catalyzed by MoO_2-complexes (0.01 mmol) in 10 mL water at 85 °C.
[b]The yield percentages derived from GC–MS results (%).
[c]TON (turnover number) = ratio of mmoles of the product (here oxide) to the mmoles of catalyst.
[d]TOF (turnover frequency) (TON/h) are shown in parentheses (mmoles (mmoles catalyst)$^{-1}$ h^{-1}).
[e]Other unknown side products are (%).

of the less polar catalyst, MoO_2L1 with more organic nature,[64] compared to that MoO_2L2 with an aqueous H_2O_2. Particularly, the catalytic reactivity of MoO_2L2 in the (ep)oxidation reactions was little inhibited with *t*BuOOH. The miscibility of the high polar catalyst with *t*BuOOH could diminish its reactivity towards the formation of oxo−/peroxomolybdenum complex intermediate catalyst.[65]

Generally, most of the catalytic (ep)oxidation systems are mainly sensitive and substantial to the catalyst type and its nature, *i.e.* the type of metal ion and the attached ligand.[66] So, from the catalytic results, it was clear that the side substituent group as a polar group (Na^+ SO_3^-—)[64,67] of the coordinated ligands played the most important role in the variation of the catalytic behavior of MoO_2L1 and MoO_2L2 in the (ep)oxidation of 1,2-cyclooctene, benzyl alcohol and thiophene in water, as reported from TONs and TOFs values in Table 4 using the most eco-friendly oxidant (H_2O_2) and in Table 5 within *t*BuOOH oxidant. Moreover, the high observable catalytic reactivity of the current homo-binuclear *cis*-MoO_2-complexes could be related to the synergic effect of

two central metal ions in their complex catalysts.[29] The synergic effect of two central metal ions could promote the oxygen transfer process in the mechanistic pathway of the (ep)oxidation reactions form the oxidant molecule to the central metal ion (Scheme 2).[68] Free radical (ep) oxidation processes could not be taken into account here due to the indicating test of diphenylamine performed that the catalytic reactions could be carried with the radical mechanistic pathway.[69] Based on the literature, the oxygen transfer process could be progressed in the presence of a coordinated solvent molecule in the catalyst,[37] in which the oxidant molecule may replace the solvent molecule (water or methanol, ROH) and then bond to the central metal ion (A) in order to generate an active oxo−/peroxomolybdenum complex intermediates,[70] as shown in Schemes 2 and 3. Both mechanistic pathways could help to understand the difference in the catalytic efficiency between H_2O_2 and *t*BuOOH for the same catalytic (ep)oxidation reaction. Bonding of the oxidant (H_2O_2 or *t*BuOOH) to the Mo-catalyst could be observed experimentally due to the little change in the color of the catalyst in the reaction media after mixing with the oxidant[29] awarding the first active intermediate (B in Schemes 2 and 3). The μ-oxo−/peroxomolybdenum intermediate (C in Scheme 2) could be formed with the attack of H_2O_2 only.[60] On the other hand, the reaction of *t*BuOOH with MoO_2-catalyst could afford peroxomolybdenum intermediate (B, Scheme 3) through the bonding to the β-oxygen of *t*BuOOH to the central metal ion,[58] as $tBuOO^-$ anion to the Lewis acidic Mo^{VI} ion.[42,71] The bonded $tBuOO^-$ to Mo^{VI} ion caused migration of H^+ of the oxidant to the *cis*-terminal oxygen of Mo = O species giving peroxointermediate C (in Scheme 3). This was studied previously with new

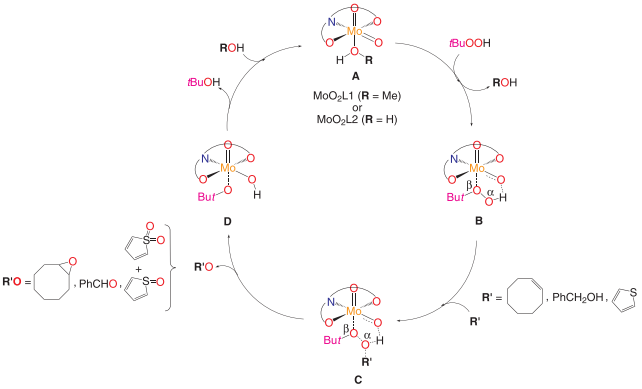

SCHEME 3 The proposed mechanistic pathway of the (ep) oxidation of 1,2-cyclooctene, benzyl alcohol and thiophene catalyzed by MoO_2L1 or MoO_2L2 using *t*BuOOH

cyclopentadienyl molybdenum imidazo[1,5-a]pyridine-3-ylidene complexes in the olefin epoxidation using *t*BuOOH.[72] It was followed by the approach of the substrate, as an electron-rich or as a nucleophile (1,2-cyclooctene, benzyl alcohol and thiophene) to the intermediate C to generate intermediate D.[73] The intermediate D caused oxidation of the substrate with the oxygen transfer process to liberate the chemoselective oxyproduct and the regenerated catalyst (A) with the formation of H_2O in the case of using H_2O_2 and *t*BuOH in the case of using *t*BuOOH.

The differences in the formed intermediate using H_2O_2 or *t*BuOOH with Mo-catalyst, as μ-oxo−/peroxomolybdenum intermediate or peroxointermediate, respectively, aimed to illustrate the variation in the yield percentages of the chemoselectives and in the efficiency of the applied Mo-catalysts.

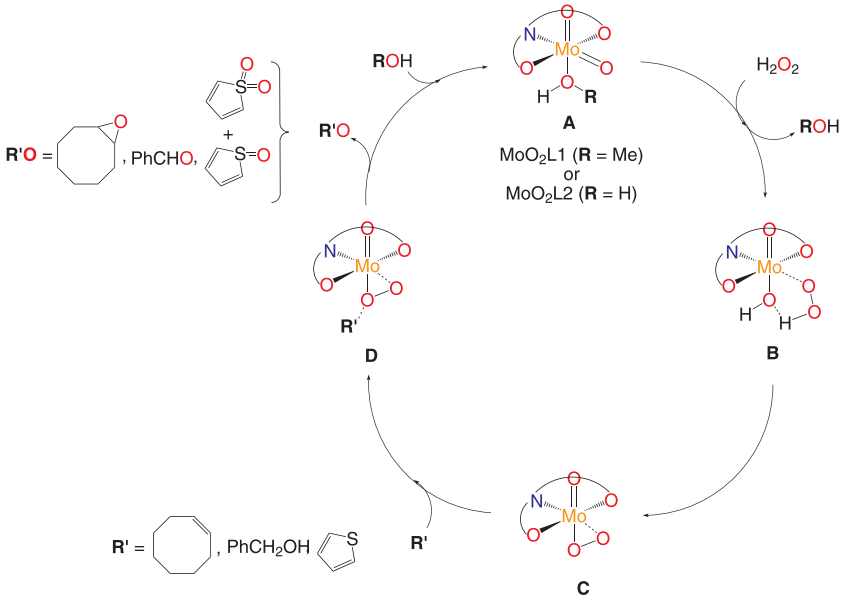

SCHEME 2 The proposed mechanistic pathway of the (ep)oxidation of 1,2-cyclooctene, benzyl alcohol and thiophene catalyzed by MoO_2L1 or MoO_2L2 using H_2O_2

3.5 | Molecular docking studies

Molecular docking is a valuable tool used to explore and explain the possible anticancer and antimicrobial mode of action(s) of different bioactive molecules. In this context, the molecular docking of H_2L1, H_2L2, MoO_2L1 and MoO_2L2 was performed using MOE package version 2019.0101 in order to investigate their binding mode to ctDNA with respect to their energy. The binding energy ($E_{conf.}$) of H_2L1, H_2L2, MoO_2L1 and MoO_2L2 with ctDNA and their final score function (S) were calculated and displayed in Table 6. The total hydrophobic surface area and the number of hydrogen bonding of H_2L1-, H_2L2-, MoO_2L1- and MoO_2L2-ctDNA of the docked structures are shown in Figure 5. The docked structures, as shown in Figure 5, suggested the possible formation of different types of hydrogen bonding between H_2L1, H_2L2, MoO_2L1 and MoO_2L2 with B-DNA, providing the binding energy and binding score magnitudes with hydrophobic interaction character.

Indeed, the negative magnitudes of the binding energy were found in the range of −603.3815 and −932.8271 kcal mol^{-1} and the binding score was in the range of −6.0514 and − 4.9293. The hydrophobic high surface area was in the range of 3651.593 and 474.8554. The former suggested a strong binding ability of the current reagents with ctDNA, *via* non-covalent stacking interactions. Accordingly, the docking studies referred to the possible different types of the formed hydrogen bonding between the current reagents and ctDNA. Hence, a hydrogen bond could be formed between H_2L1 (phenolic hydroxyl group) and the ctDNA (DG16) with a bond distance of 3.18 Å. Additionally, two other hydrogen bonds could also be formed between the water molecule and the two hydrazone NH-groups of H_2L1 with bond distances 3.02 and 3.06 Å, respectively. For H_2L2, two hydrogen bonds could be formed between the labile water molecule and the hydrazone NH—groups of H_2L2 with bond distances 2.99 and 3.17 Å, respectively. The docking results assigned the formation of one hydrogen bond between MoO_2L1 and MoO_2L2 with the guanine (DG14) and the adenine (DA18) bases of the ctDNA with bond distances of 3.33 and 2.91 Å, respectively. Moreover, there was a π–hydrogen interaction in MoO_2L2 with a bond distance of 4.66 Å.

Interestingly, the molecular docking obtains showed that the polar *p*-sodium sulfonate group substituent in MoO_2L2 had an obvious role in binding with ctDNA (Figure 5), besides the hydrogen bonding of the labile coordinated H_2O molecules. The molecular docking studies illustrated that the hydrogen bond(s) and the hydrophobic interaction of MoO_2L1 and MoO_2L2 played an essential role in the binding interaction. Accordingly, the interaction of the MoO_2-complexes with ctDNA was probably grooved binding. These interesting results need more studies and further investigations such as DNA binding studies employing spectroscopic and viscosity experiments, as shown below.

3.6 | DNA binding studies

3.6.1 | Absorption spectral studies

The most prominent spectral characteristics of the ctDNA double-helix after reaction with other molecules is hyperchromism and hypochromism.[9] The later could be formed from the stabilization of the ctDNA duplex either *via* the electrostatic effect or the intercalative binding mode. On the other hand, hyperchromism could be formed from the splitting of the ctDNA duplex.[74] Therefore, the binding capacity of the ctDNA with the MoO_2-complexes (MoO_2L1 and MoO_2L2) was estimated *via* the evaluation of their electronic spectral changes after their interaction with ctDNA. The absorption spectrum of

TABLE 6 The molecular docking calculated values for H_2L1 and H_2L2, and their *cis*-MoO_2-complexes

Comp.	No. of Hydrogen bonds	Interacting nucleotide	Distances ()	E (Kcal/mol)	Total hydrophobic surface area	k_b	S	$E_{conf.}$
H_2L1	1	DG16	3.02	−2.6	365.1593	5.51	−6.0514	−976.9422
	2	H_2O	3.06	−0.5				
	3	H_2O	3.18	−0.9				
H_2L2	1	H_2O	2.99	−2.7	251.6536	5.10	−5.8617	−932.8271
	2	H_2O	3.17	−0.5				
MoO_2L1	1	DG14	3.33	−2.4	474.8554	4.56	−4.9293	−603.3815
MoO_2L2	1	DA18	2.91	−2.5	262.7468	5.27	−5.9698	−944.2164
	π-H	DC11	4.66	−0.6				

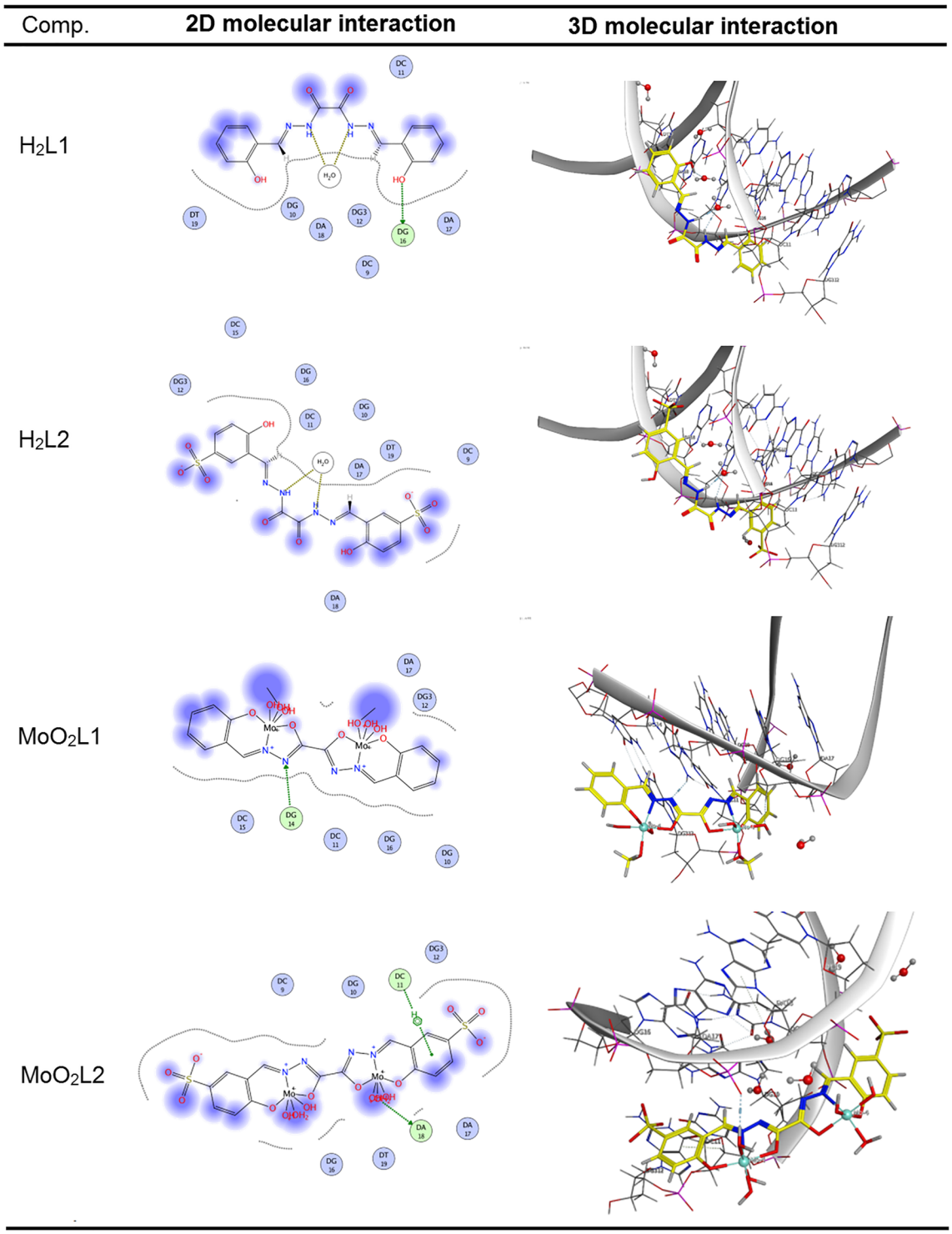

FIGURE 5 Molecular docking interaction mode of H_2L1, H_2L2, MoO_2L1 and MoO_2L2 with ctDNA

MoO_2L1 and MoO_2L2 in the absence and presence of ctDNA is presented in Figures 6 and 7.

After the gradual addition of ctDNA, the band of MoO_2L1 complex at 500 nm and MoO_2L2 complex at 246 exhibited a weak hypochromic effect of 7.71% (bathochromism of 11 nm) and 2.46% (bathochromism of 8 nm), respectively. The obtained spectral data suggested a stacking interaction binding mode between the ctDNA base pairs and the aromatic chromophore of the MoO_2-complexes. The small red-shift in the bands of the MoO_2-complexes proposed a hypochromism. This also beholds an intercalative binding mode of the MoO_2-complexes through their interaction with ctDNA. The intrinsic binding constant (K_b), as deduced in the

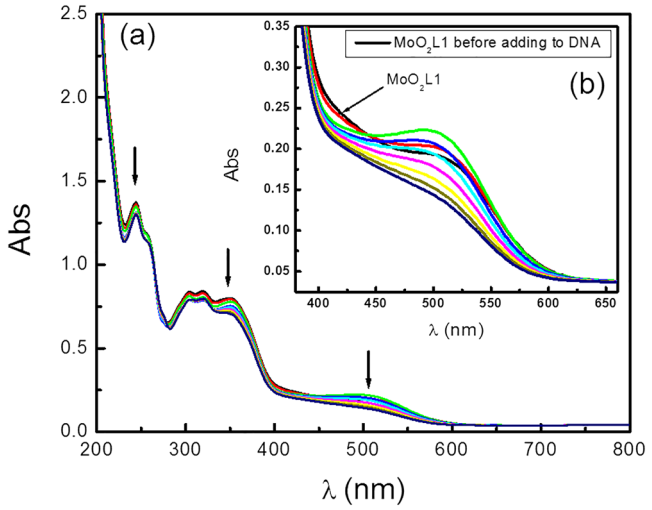

FIGURE 6 The UV–Vis. spectral scans of MoO_2L1 in the buffer solution in the absence and presence of ctDNA with interval time 15 min (a); the visible zoom of the electronic spectra of MoO_2L1 in absence and presence of ctDNA (b)

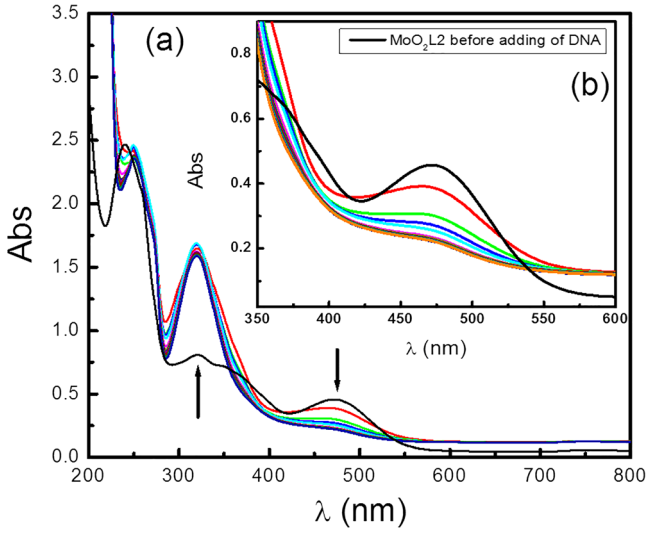

FIGURE 7 The UV–Vis. spectral scans of MoO_2L2 in the buffer solution in the absence and presence of ctDNA with interval time 15 min (a); the visible zoom of the electronic spectra of MoO_2L2 in absence and presence of ctDNA (b)

experimental section, was used for comparing the quantitative affinity of ctDNA binding to the studied MoO_2-agents. The intrinsic binding constants K_b were also involved to determine quantitatively the extent of the binding strength of the MoO_2-complexes. As depicted in Table 7, the K_b values for MoO_2L1 and MoO_2L2 are 4.83 $\times 10^5$ and 7.28 $\times 10^5$ M^{-1}.

The obtained results of DNA-binding and K_b values of the current MoO_2-complexes, as dihydrazone reagents, afforded more distinguished reactivity towards DNA compared to those previously studied hydrazone reagents towards similar cell lines.[4,51]

3.6.2 | Hydrodynamic measurements & viscosity measurements

Emission and absorption experiments provide additional helpful information about the expected intercalative binding mode with ctDNA.[75] Viscosity measurements were therefore performed to further explain the interactive nature between the *cis*-MoO_2-complexes (MoO_2L1 and MoO_2L2) and ctDNA. The ctDNA viscosity is expected to be increased after intercalation. On the other hand, ctDNA viscosity could be reduced in *non*-classical, partial or intercalation due to bending of the ctDNA helix.[76] Ethidium bromide was applied as a reference in such experimental work. As shown in Figure 8, the relative viscosity of ctDNA was significantly enhanced in the case of ethidium bromide. Similarly, the viscosity of ctDNA improved steadily within increasing the amounts of MoO_2-complexes, however; the viscosity increase extent with EB was significantly more. The increased degree of viscosity of ctDNA within MoO_2L2 was greater than that with MoO_2L1. Conclusively, the UV-absorption and viscosity measurement results suggested that the binding mode of *cis-bis*-dioxomolybdenum complexes involves base-pair intercalation which was in agreement with the molecular docking studies.

3.7 | Biological evaluation

3.7.1 | Anticancer activity evaluation

The antiproliferative potential of H_2L1, H_2L2, MoO_2L1 and MoO_2L2 was examined using HCT-116, MCF-7 and HepG2 cell lines and the IC_{50} values were determined and recorded in Table 8. *Bis*-dioxomolybdenum complexes (MoO_2L1 and MoO_2L2) exhibited superior cytotoxicity against all the three applicable cell lines comparing to their corresponded free *bis*-Schiff base ligands (H_2L1 and H_2L2) (Figure S23). The enhancement of their anticancer potential, for the reacting free ligands, could be related to their various structural features and would be attributable to redox-active molybdenum (VI) ions.[77,78]

In general, the viability of HCT-116, MCF-7 and HepG2 cells, which treated with the test current reagents, decreased in a concentration-dependent manner, however, the anticancer activity of those studied reagents (MoO_2-complexes and their free ligands) was less than the standard drug, vinblastine (Table S3). All the probed reagents were more cytotoxic against the MCF-7 cell line

TABLE 7 Spectral parameters for the interaction of *cis*-MoO_2-complexes with ctDNA

Complex	λ_{max} free (nm)	λ_{max} bound (nm)	Δn	Chromism (%)	Type of Chromism	Binding constant[a] × 10^5	ΔG KJ mol^{-1}
MoO_2L1	248	240	0	4.99	Hyper	4.83	−33.31
	300	300	0	5.27			
	321	321	0	5.52			
	359	358	−1	6.75			
	500	511	11	7.71			
MoO_2L2	246	254	8	2.46	Hypo	7.26	−36.45
	318	318	0	12.05			
	475	469	−6	6.38			

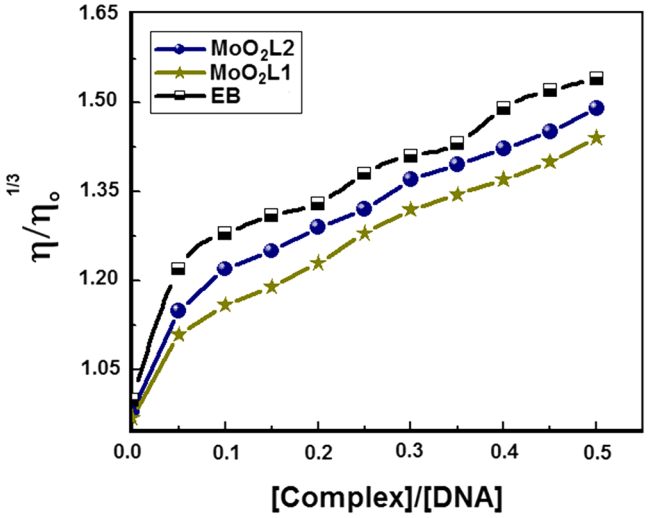

FIGURE 8 Effect of the increased amounts of MoO_2-complexes on the relative viscosities of ctDNA at [DNA] = 0.5 mM and 25 °C

TABLE 8 Influence of H_2L1, H_2L2, MoO_2L1, and MoO_2L2 on the viability of HCT-116, HepG2, and MCF-7 cells

	IC_{50} (μM)[b]		
Comp.[a]	HCT-116	MCF-7	HepG-2
H_2L1	98.40	78.20	87.50
H_2L2	113.50	84.30	95.70
MoO_2L1	17.50	8.90	14.50
MoO_2L2	25.60	13.20	17.90
Vinblastine	13.3	4.12	7.50

The metabolic activity of the cells was estimated after 48 hr of incubation with different concentrations of the investigated compounds by means of an MTT assay.

[a]The IC_{50} value was determined from the dose–response curves as the mean of two parallel experiments.

[b]Fluorouracil (5-Fu) was used as a positive control; Selectivity index (SI) is the ratio of the IC_{50} value for normal cells (WI-38) to the IC_{50} values for HepG2 and MCF-7 cells; No growth inhibition was recorded.

and MoO_2L1 presented the lowest IC_{50} values. Therefore, MoO_2L1 considered to be the most potent among all the tested compounds. Noteworthy, MoO_2L2 and H_2L2 bearing the hydrophilic sodium sulfonate group displayed lower anticancer activities compared to their analogs MoO_2L1 and H_2L1, respectively. This may be due to its poor lipophilic nature, as observed elsewhere.[4]

3.7.2 | Antioxidant

DPPH assay

Since the *bis*-dioxomolybdenum complexes (MoO_2L1 and MoO_2L2) displayed promising anticancer potential and good ctDNA binding capability, the reducing abilities of these current compounds were further estimated *via* the DPPH assay (Table 9). The deep violet radical 1,1-diphenyl-2-picryl-hydrazine was formed by the reaction of antioxidants with DPPH. The former had a strong absorption band at 517 nm.[46,47] The assay relied on the absorption disappearance and decolorization due to electron pairing in the presence of free radical scavengers. In particular, the reaction was stoichiometric to the number of electrons taken up. Methanol was used as a blank, whereas, DPPH solution was applied as the negative control without the tested reacting compounds. The scavenging activity percentages (%), which referred to the free radical DPPH activity, was determined by that equation: inhibition % = [(Absorbance of control − Absorbance of the test sample)/Absorbance control] × 100.

Consequently, the *cis*-MoO_2-complexes, MoO_2L1 and MoO_2L2, demonstrated moderate free radical-scavenging activity compared to vitamin C, as reported in Table 9.

SOD assay

The formation of most ROS (*e.g.* singlet oxygen, hydrogen peroxide and hydroxyl radical) could rely on the $O_2^{\cdot-}$

TABLE 9 Evaluation of the antioxidant activity of *cis*-MoO_2-complexes (MoO_2L1 and MoO_2L2) using the DPPH and SOD assays

	DPPH assay	SOD assay	
Complex	Radial scavenging (%)	ΔOD_{560} (5 min)	Inhibition (%)
MoO_2L1	56	0.52	89
MoO_2L2	61	0.59	97
Vitamin C	89.6	--[a]	--[a]
Control	--[a]	0.516	--[a]
HR SOD	--[a]	0.163	68.42

[a]Absorbance was not recorded.

formation for antioxidant studies.[77] Antioxidants could diminish the production of $O_2^{\cdot-}$, and in this way, it is possible to evaluate the superoxide anion scavenging effect of different examined ligands and their corresponding metal complexes. The activity of superoxide dismutase (SOD) was explored in the absence and presence of MoO_2L1 and MoO_2L2, spectrophotometrically with SOD kit.[61] The $O_2^{\cdot-}$ scavenging capabilities of the agents in terms of inhibition % efficiency could be obtained in Table 9. The obtained results showed that the MoO_2L2 complex had a higher inhibition effect (97%) than that of MoO_2L1 (89%). Both MoO2-complexes illustrated respectable superoxide anion scavenging activity compared to the reported MoO_2-hydrazone complexes.[4]

3.7.3 | Antimicrobial activity assessment

The promising catalytic, anticancer and antioxidant features of the newly synthesized *bis*-dioxomolybdenum complexes (MoO_2L1 and MoO_2L2) and their corresponding *bis*-dihydrazone ligands (H_2L1 and H_2L2) encouraged us to examine their corresponding antimicrobial potentials. Several transition metal complexes,[79] specifically *bis*-dioxomolybdenum complexes,[4,80] were reported as selective suppressors of different microbial action. Therefore, the antimicrobial activity of the MoO_2-complexes and their free ligands under considerations was examined using the disc diffusion and microdilution methods against *Staphylococcus aureus* Gram-positive bacteria and two Gram-negative bacteria namely, *Escherichia coli* and *Serratia Marcescence* as well as *Candida albicans*, *Aspergillus flavus* and *Trichophyton rubrum* fungal strains. The results are depicted in Table 10. The antimicrobial data were compared using the standard antibiotics, ofloxacin (for bacteria) and fluconazole (for fungi) and their corresponding % activity index have been also listed in Table 10. The inhibition zones were the clear zones around the discs, which were measured in mm.

Intriguingly, it was observed that all the *cis*-bis-dioxomolybdenum complexes revealed more obvious antimicrobial activities than their corresponding free ligands under identical experimental conditions against the same organisms.[4,8,9] For the four examined compounds, MoO_2L1 strongly hampered the growth of the bacterial and fungal strains. It was also worthwhile to mention that MoO_2L2 and H_2L2 bearing the hydrophilic sulfonate group displayed lower antimicrobial activity compared to their analogs MoO_2L1 and H_2L1, respectively. This could be attributable to their poor lipophilicity. Furthermore, the current compounds were thereafter selected for MIC studies (Table 11) and results were in good agreement with the disc diffusion method assay. The MIC of MoO_2-complexes and their free ligands

TABLE 10 Antimicrobial agar diffusion assay of H_2L1, H_2L2, and their corresponding *cis*-MoO_2-complexes: diameters (mm) of inhibition zones (% of standard) after one day

	Diameter inhibition zone in mm (% activity index)					
	Bacteria[a]			*Fungi*[a]		
Comp.	*Serratia Marcescence*	*Escherichia coli*	*Micrococcus Luteus*	*Aspergillus flavus*	*Getrichm candidum*	*Fusarium oxysporum*
H_2L1	11(39)	9(41)	14(36)	9(41)	16(41)	11(42)
H_2L2	9(32)	7(32)	11(28)	7(32)	14(36)	9(35)
MoO_2L1	26(93)	21(96)	38(97)	21(95)	37(95)	25(96)
MoO_2L2	24(86)	19(86)	35(90)	17(77)	34(87)	22(85)
Ofloxacin	28(100)	22(100)	39(100)	b	b	b
Fluconazole	b	b	b	22(100)	39(100)	26(100)

[a]Diameters (mm) of zones of inhibition (agar diffusion assay) are provided. In each case, 6 mm disks with 20 μM of the test compounds were incubated. Ofloxacin and fluconazole were used as positive control.
[b]Values refer either to not detected or inactive.

TABLE 11 Minimum inhibitory concentration (MIC/μM) for the antimicrobial assay of H_2L1, H_2L2, and their *cis-bis*-dioxomolybdenum complexes

	Minimum Inhibition concentration (MIC) μM					
Comp.	***Serratia Marcescence***	***Escherichia coli***	***Micrococus Luteus***	***Aspergillus flavus***	***Getrichm candidum***	***Fusarium oxysporum***
H_2L1	5.50	7.50	6.25	6.00	8.00	6.75
H_2L2	6.50	8.00	7.00	7.25	8.50	7.50
MoO_2L1	3.50	5.00	4.25	4.25	5.50	4.75
MoO_2L2	4.25	6.00	4.75	5.00	6.75	5.75

varied from 8.5 to 3.5 μM (Figure S24 in the supplementary materials).

The superior biological activity of the MoO_2-complexes compared to their corresponding dihydrazone free ligands could be explained using the Tweedy's chelation theory and Overtone's concept.[78] After chelation, the molybdenum atom lipophilicity was enhanced due to the increase of π-electrons delocalization over the complex sphere. Such behavior could favor the diffusion through the cell membrane. On the other hand, the polarity of molybdenum ion is extremely decreased due to the partial sharing of its positive charge and overlapping of the dihydrazone ligand orbital with donor groups.[81]

There are many other factors for the superior bioactivity of metal complexes compared to their free ligands and these include pharmacokinetics, dipole moment, conductivity, solubility and steric factors. However, more intensive studies need to be made in order to identify their biological pathways. Furthermore, the week biological activity of MoO_2L2 and H_2L2 is due to the presence of the polar sulfonate group, which in turn decreases their corresponding lipophilicity and hence hampers their diffusion through the cell membrane. The obtained assigned more antimicrobial potential of the current compounds more than those previously studied hydrazone reagents of the similar cell membrane.[4,8,9]

4 | CONCLUSIONS

Two *bis*-tridentate oxalylsalicylidenedihydrazone Schiff-bases, H_2L1 and H_2L2, were prepared by the reaction of oxalyldihydrazide with suitable salicylaldehyde derivatives. The reaction of *cis*-$MoO_2(acac)_2$ with H_2L1 and H_2L2 afforded the corresponding *bis*-dioxomolybdenum complexes MoO_2L2 and MoO_2L2. The structures of MoO_2L2 and MoO_2L2 were confirmed by EA, ultraviolet–visible, mass spectra and FT-IR, as well as, ^{1}H- and ^{13}C-NMR spectra. MoO_2L1 and MoO_2L2 concerned as considerable active homogeneous catalysts in the selective (ep)oxidation of 1,2-cyclooctene, benzyl alcohol and thiophene using an aqueous H_2O_2 or *tert*-butyl hydroperoxide (*t*BuOOH) at 85 °C. The *p*-sodium sulfonate group shows an appreciable influence by improving the catalytic efficiency of MoO_2L2 compared to MoO_2L1 (in absence of *p*-$NaSO_3$-group).

Both MoO_2L1 and MoO_2L2 interacted with ctDNA by intercalative binding mode, which have been proven using molecular modeling and DNA binding studies. Both studies proposed that the binding mode of *cis*-MoO_2-complexes involves base-pair intercalation.

The antiproliferative activity of H_2L1, H_2L2, MoO_2L1 and MoO_2L2 was evaluated using different cancer cell lines including HCT-116, MCF-7, and HepG2 cells. MoO_2L1 and MoO_2L2 showed improved cytotoxic potentials in tested three cell lines compared to their corresponding free *bis*-Schiff base ligands (H_2L1 and H_2L2). Furthermore, the free radical scavenging abilities of the current compounds were further estimated by their strong interaction with the free stable radical DPPH. MoO_2L1 and MoO_2L2 showed moderate free radical-scavenging activity compared to ascorbic acid and good superoxide anion scavenging activity. The *bis*-dioxomolybdenum complexes manifested higher antimicrobial activities than that of the free ligands (*bis*-Schiff bases) under identical experimental conditions against the same organisms.

ACKNOWLEDGEMENTS

This study was received funding from the Deanship of Scientific Research, King Faisal University, Al-Ahsa under the grant number 110143.

ORCID

Mohamed Shaker S. Adam https://orcid.org/0000-0001-8826-3558

REFERENCES

[1] a) G. Schwarz, R. R. Mendel, M. W. Ribbe, *Nature* **2009**, *460*, 839; b) G. Moula, M. Bose, S. Sarkar, *Inorg. Chem.* **2013**, *52*, 5316; c) J. Mitra, S. Sarkar, *Dalton Trans.* **2013**, *42*, 3050; d) A. Majumdar, S. Sarkar, *Coord. Chem. Rev.* **2011**, *255*, 1039.

[2] a) C. M. Cordas, J. J. Moura, *Coord. Chem. Rev.* **2019**, *394*, 53; b) J. A. Hernandez, S. J. George, L. M. Rubio, *Biochemistry* **2009**, *48*, 9711; c) R. R. Mendel, F. Bittner, *Biochim. Biophys. Acta (BBA)-Mol. Cell Res.* **2006**, *1763*, 621.

[3] a) C. M. Da Silva, D. L. da Silva, L. V. Modolo, R. B. Alves, M. A. de Resende, C. V. Martins, A. de Fátima, *J. Adv. Res.* **2011**, *2*, 1; b)L. Shi, H. M. Ge, S. H. Tan, H. Q. Li, Y. C. Song, H. L. Zhu, R. X. Tan, *Eur. J. Med. Chem.* **2007**, *42*, 558.

[4] M. S. S. Adam, O. M. El-Hady, F. Ullah, *RSC Adv.* **2019**, *9*, 34311.

[5] (a)S. Gupta, M. V. Kirillova, M. F. C. G. da Silva, A. J. L. Pombiero, A. M. Kirillov, *Inorg. Chem.* **2013**, *52*, 8601. (b)H. H. Monfared, R. Bikas, P. M. Anarjan, A. J. Blake, V. Lippolis, N. B. Arslan, C. Kazak, *Polyhedron* **2014**, *69*, 90. (c)R. Borthakur, A. Kumar, R. A. Lal, *Spectrochim. Acta a* **2015**, *149*, 621. (d)R. Borthakur, U. Thapa, M. Asthana, S. Mitra, K. Ismail, R. A. Lal, *J. Photochem. Photobiol. A* **2015**, *301*, 6.

[6] (a)H. H. Monfared, N. A. Lalami, A. Pazio, K. Wozniak, C. Janiak, *Inorg. Chim. Acta* **2013**, *406*, 241. (b)C. Das, P. Adak, S. Mondal, R. Sekiya, R. Kuroda, S. I. Gorelsky, S. K. Chattopadhyay, *Inorg. Chem.* **2014**, *53*, 11426. (c) P. Paciorek, J. Szklarzewicz, A. Jasinska, B. Trzewik, W. Nitek, M. Hodorowicz, *Polyhedron* **2015**, *87*, 226. (d)T. Sedaghat, M. Aminian, G. Bruno, H. A. Rudbari, *J. Organomet. Chem.* **2013**, *737*, 26. (e)S. Roy, T. N. Mandal, A. K. Barik, S. Pal, R. J. Butcher, M. S. E. Fallah, J. Tercero, S. K. Kar, *Dalton Trans.* **2007**, *12*, 1229.

[7] (a)S. Shahzadi, S. Ali, S. K. Sharma, K. Qanungo, *J. Iran. Chem. Soc.* **2010**, *7*, 419. (b)C. G. Young, *Eur. J. Inorg. Chem.* **2016**, *12*, 2357. (c)P. V. Bernhardt, *Chem. Commun.* **2011**, *47*, 1663.

[8] (a)L. H. Abdel-Rahman, A. M. Abu-Dief, M. Ismael, M. A. A. Mohamed, N. A. Hashem, *J. Mol. Struct.* **2016**, *1103*, 232. (b)L. H. Abdel-Rahman, N. M. Ismail, M. Ismael, A. M. Abu-Dief, E. A. Ahmed, *J. Mol. Struct.* **2017**, *1134*, 851.

[9] (a)L. H. Abdel-Rahman, A. M. Abu-Dief, R. M. El-Khatib, S. M. Abdel-Fatah, *Bioorg. Chem.* **2016**, *69*, 140. (b)A. M. Abu-Dief, I. F. Nassar, W. H. Elsayed, *Appl. Organomet. Chem.* **2016**, *30*, 917. (c)L. H. Abdel-Rahman, A. M. Abu-Dief, M. O. Aboelez, A. A. H. Abdel-Mawgoud, *J. Photochem. Photobiol. B.* **2017**, *170*, 271. (d)L. H. Abdel-Rahman, M. S. S. Adam, A. M. Abu Dief, H. Moustafa, M. T. Basha, A. S. Aboraia, H. E. Ahmed, *Appl. Organomet. Chem.* **2018**, *32*, e4527.

[10] (a)L. Krivosudský, P. Schwendt, R. Gyepes, Z. Zák, *Polyhedron* **2014**, *81*, 421. (b)L. Krivosudský, P. Schwendt, J. Šimunek, R. Gyepes, *J. Inorg. Biochem.* **2015**, *147*, 65.

[11] (a)J. C. Pessoa, *J. Inorg. Biochem.* **2015**, *147*, 4. (b)L. Lu, J. Yue, C. Yuan, M. Zhu, H. Han, Z. Liu, M. Guo, *J. Inorg. Biochem.* **2011**, *105*, 1323.

[12] (a)Z. Kazemi, H. A. Rudbari, M. Sahihi, V. Mirkhani, M. Moghadam, S. Tangestaninejad, I. Mohammadpoor-Baltork, S. Gharaghani, *J. Photochem. Photobiol. B.* **2016**, *162*, 448. (b)A. Rauf, A. Shah, A. A. Khan, A. H. Shah, R. Abbasi, I. Z. Qureshi, S. Ali, *Spectrochim. Acta A* **2017**, *176*, 155. (c) A. K. Saini, P. Kumari, V. Sharma, P. Mathur, S. M. Mobin, *Dalton Trans.* **2016**, *45*, 19096.

[13] (a)Y.-T. Liu, J. Sheng, D.-W. Yin, H. Xin, X.-M. Yang, Q.-Y. Qiao, Z.-J. Yang, *J. Organomet. Chem.* **2018**, *856*, 27. (b) C. M. Sharaby, M. F. Amine, A. A. Hamed, *J. Mol. Struct.* **2017**, *1134*, 208.

[14] (a)W. H. Mahmoud, N. F. Mahmoud, G. G. Mohamed, *Appl. Organomet. Chem.* **2017**, *31*, e3858. (b) W. H. Mahmoud, R. G. Deghadi, M. M. I. El Desssouky, G. G. Mohamed, *Appl. Organomet. Chem.* **2018**, *32*, e4556. (c)W. H. Mahmoud, M. M. Omar, F. N. Sayed, G. G. Mohamed, *Appl. Organomet. Chem.* **2018**, *32*, e4386. (d)W. H. Mahmoud, R. G. Deghadi, G. G. Mohamed, *Res. Chem. Intermed.* **2016**, *42*, 7869.

[15] (a)R. Rasool, S. Hasnain, *Spectrochim. Acta A* **2015**, *148*, 435. (b)A. A. M. Belal, I. M. El-Deen, N. Y. Farid, R. Zakaria, M. S. Refat, *Spectrochim. Acta A* **2015**, *149*, 771.

[16] (a)E. M. Zayed, A. M. M. Hindy, G. G. Mohamed, *Appl. Organomet. Chem.* **2018**, *32*, e3952. bE. M. Zayed, G. G. Mohamed, W. M. I. Hassan, A. K. Elkholy, H. Moustafa, *Appl. Organomet. Chem.* **2018**, *32*, e4375. cE. M. Zayed, M. A. Zayed, A. M. M. Hindy, G. G. Mohamed, *Appl. Organomet. Chem.* **2018**, *32*, e4603.

[17] (a)M. Shebl, *J. Mol. Struct.* **2017**, *1128*, 79. (b)G. S. Hegde, S. P. Netalkar, V. K. Revankar, *Appl. Organomet. Chem.* **2019**, *33*, e4840. (c)M. Shebl, M. A. El-ghamry, S. M. E. Khalil, M. A. A. Kishk, *Spectrochim. Acta a* **2014**, *126*, 232.

[18] M. Shebl, S. M. E. Khalil, M. A. A. Kishk, D. M. EL-Mekkawi, M. Saif, *Appl. Organomet. Chem.* **2019**, *33*, e5147.

[19] (a)I. Syiemlieh, A. Kumar, S. D. Kurbah, R. A. Lal, *J. Mol. Struct.* **2018**, *1166*, 252. (b)I. Syiemlieh, A. Kumar, S. D. Kurbah, A. K. De, R. A. Lal, *J. Mol. Struct.* **2018**, *1151*, 343.

[20] (a)T. G. Jo, J. J. Lee, E. Nam, K. H. Bok, M. H. Lim, C. Kim, *New J. Chem.* **2016**, *40*, 8918. (b)W. Al Zoubi, N. Al Mohanna, *Spectrochim. Acta A* **2014**, *132*, 854.

[21] (a)B. D. Wang, Z. Y. Yang, P. Crewdson, D. Q. Wang, *J. Inorg. Biochem.* **2007**, *101*, 1492. (b)C. D. Fan, H. Su, J. Zhao, B. X. Zhao, S. L. Zhang, J. Y. Miao, *Eur. J. Med. Chem.* **2010**, *45*, 1438. (c)S. Pasayat, S. P. Dash Saswati, P. K. Majhi, Y. P. Patil, M. Nethaji, H. R. Dash, S. Das, R. Dinda, *Polyhedron* **2012**, *38*, 198. (d)J. V. Ragavendran, D. Sriram, S. K. Patel, I. V. Reddy, N. Bharathwajan, J. Stables, P. Yogeeswari, *Eur. J. Med. Chem.* **2007**, *42*, 196.

[22] (a)P. Liang, Y. Liu, L. Guo, *J. Anal. At. Spectrom.* **2004**, *19*, 1006. (b)Y. C. Sun, J. Y. Yang, S. R. Tzeng, *Analyst* **1999**, *124*, 421.

[23] A. W. Jeevadason, K. K. Murugavel, M. A. Neelakantan, *Renew. Sustain. Energy Rev.* **2014**, *36*, 220.

[24] (a)M. S. S. Adam, H. Elsawy, *J. Photochem. Photobiol. B.* **2018**, *184*, 34. (b)M. S. S. Adam, M. M. Youssef, M. F. Abo Elghar, A. M. Hafez, U. El-Ayaan, *Appl. Organomet. Chem.* **2017**, *31*, e3650.

[25] (a)P. G. Cozzi, *Chem. Soc. Rev.* **2004**, *33*, 410. (b)W. Zhao, C. Yang, Z. Cheng, Z. Zhang, *Green Chem.* **2016**, *18*, 995. (c) X. Lang, X. Chen, J. Zhao, *Chem. Soc. Rev.* **2014**, *43*, 473.

[26] (a)T. J. Korstanje, E. Folkertsma, M. Lutz, J. T. B. H. Jastrzebski, R. J. M. K. Gebbink, *Eur. J. Inorg. Chem.* **2013**, *2013*, 2195. (b)T. C. R. Rocha, A. Oestereich, D. V. Demidov, M. Havecker, S. Zafeiratos, G. Weinberg, V. I. Bukhtiyarov, A. Knop-Gericke, R. Schlogl, *Phys. Chem.*

Chem. Phys. **2012**, *14*, 4554. (c)M. R. Maurya, B. Uprety, F. Avecilla, *Eur. J. Inorg. Chem.* **2016**, *2016*, 4802.

[27] (a)M. Raynal, P. Ballester, A. Vidal-Ferran, P. W. N. M. Leeuwen, *Chem. Soc. Rev.* **2014**, *43*, 1660. (b)Z. Chen, B. Wang, J. Zhang, W. Yu, Z. Liu, Y. Zhang, *Org. Chem. Front.* **2015**, *2*, 1107. (c)Z. Shi, C. Zhang, C. Tang, N. Jiao, *Chem. Soc. Rev.* **2012**, *41*, 3381. *d*C. Schulzke, *Eur. J. Inorg. Chem.* **2011**, *2011*, 1189.

[28] (a)Y. Li, F. Zaera, *Catal. Sci. Technol.* **2015**, *5*, 3773. (b) M. S. S. Adam, *Appl. Organomet. Chem.* **2018**, *32*, e4234. (c) C. Annese, D. Caputo, L. D'Accolti, C. Fusco, A. Nacci, A. Rossin, G. Tuci, G. Giambastiani, *Eur. J. Inorg. Chem.* **2019**, *2019*, 221.

[29] (a)M. S. S. Adam, *Monatsh. Chem.* **2015**, *146*, 1823. (b) M. S. S. Adam, A. D. Mohamad, O. M. El-Hady, *Monatsh. Chem.* **2014**, *145*, 435. (c)M. S. S. Adam, H. M. Abd El-Lateef, K. A. Soliman, *J. Mol. Liq.* **2018**, *250*, 207.

[30] (a)M. R. Maurya, N. Saini, F. Avecilla, *RSC Adv.* **2015**, *5*, 101076. (b)M. R. Maurya, N. Saini, F. Avecilla, *RSC Adv.* **2016**, *6*, 12993. (c)M. R. Maurya, S. Dhaka, F. Avecilla, *Polyhedron* **2015**, *96*, 79. (d)S. Rayati, A. Ghasemi, N. Sadeghzadeh, *Cat. Com.* **2010**, *11*, 792.

[31] (a)Z. Hu, H. Fu, Y. Li, *Inorg. Chem. Commun.* **2011**, *14*, 497. (b)Y. Ln, X. Fu, B. Gong, X. You, X. Tu, J. Chen, *J. Mol. Catal. A* **2010**, *322*, 55. (c)A. Rezaeifard, I. Sheikhshoaie, N. Monadi, M. Alipour, *Polyhedron* **2010**, *29*, 2703.

[32] (a)R. Bikas, V. Lippolis, N. Noshiranzadeh, H. Farzaneh-Bonab, A. J. Blake, M. Siczek, H. Hosseini-Monfared, T. Lis, *Eur. J. Inorg. Chem.* **2017**, *2017*, 999. (b)M. Ghorbanloo, R. Bikas, G. Małecki, *Inorg. Chim. Acta* **2016**, *445*, 8. (c)D.-L. Peng, *Transition Met. Chem.* **2016**, *41*, 843.

[33] S. D. Kurbah, A. Kumar, I. Syiemlieh, M. Asthana, R. A. Lal, *Inorg. Chem. Commun.* **2017**, *86*, 39.

[34] P. Thiruvengetam, R. D. Chakravarthy, D. K. Chand, *J. Catal.* **2019**, *376*, 123.

[35] J. J. Boruah, S. P. Das, *RSC Adv.* **2018**, *8*, 34491.

[36] F. Le Quéméner, S. Barman, N. Merle, M. A. Aljuhani, M. K. Samantaray, Y. Saih, K. C. Szeto, A. De Mallmann, Y. Minenkov, K.-W. Huang, L. Cavallo, M. Taoufik, J.-M. Basset, *ACS Catal.* **2018**, *8*, 7549.

[37] M. Zare, Z. Moradi-Shoeili, M. Bagherzadeh, S. Akbayrak, S. Ozkar, *New J. Chem.* **2016**, *40*, 1580.

[38] M. Mirzaee, B. Bahramian, J. Gholizadeh, A. Feizi, R. Gholami, *Chem. Eng. J.* **2017**, *308*, 160.

[39] N. Zwettler, J. A. Schachner, F. Belaj, N. C. Mösch-Zanetti, *Mol. Catal.* **2017**, *443*, 209.

[40] G. Romanowski, J. Kira, *Polyhedron* **2016**, *117*, 352.

[41] M. M. Javadi, M. Moghadam, I. Mohammadpoor-Baltork, S. Tangestaninejad, V. Mirkhani, H. Kargar, M. N. Tahir, *Polyhedron* **2014**, *72*, 19.

[42] M. Hatefi-Ardakani, S. Saeednia, Z. Pakdin-Parizi, M. Rafeezadeh, *Res. Chem. Intermed.* **2016**, *42*, 7223.

[43] J. Morlot, N. Uyttebroeck, D. Agustin, R. Poli, *ChemCatChem* **2013**, *5*, 601.

[44] M. J. Frisch, G. W. Trucks, H. B. Schlegel, G. E. Scuseria, M. A. Robb, J. R. Cheeseman, G. Scalmani, V. Barone, B. Mennucci, G. A. Petersson, H. Nakatsuji, M. Caricato, X. Li, H. P. Hratchian, A. F. Izmaylov, J. Bloino, G. Zheng, J. L. Sonnenberg, M. Hada, M. Ehara, K. Toyota, R. Fukuda, J. Hasegawa, M. Ishid, T. Nakajima, Y. Honda, O. Kitao, H. Nakai, T. Vreven, J. A. Montgomery, J. E. Peralta, F. Ogliaro, M. Bearpark, J. J. Heyd, E. Brothers, K. N. Kudin, V. N. Staroverov, T. Keith, R. Kobayashi, J. Normand, K. Raghavachari, A. Rendell, J. C. Burant, S. S. Iyengar, J. Tomasi, M. Cossi, N. Rega, J. M. Millam, M. Klene, J. E. Knox, J. B. Cross, V. Bakken, C. Adamo, J. Jaramillo, R. Gomperts, R. E. Stratmann, O. Yazyev, A. J. Austin, R. Cammi, C. Pomelli, J. W. Ochterski, R. L. Martin, K. Morokuma, V. G. Zakr-Zewski, G. A. Voth, P. Salvador, J. J. Dannenberg, S. Dapprich, A. D. Daniels, O. Farkas, J. B. Foresman, J. V. Ortiz, J. Cioslowski, D. J. Fox, Gaussian, Inc., Wallingford CT, **2010**.

[45] T. A. Halgren, *J. Comput. Chem.* **1996**, *17*, 490.

[46] (a)S. Shaaban, A. M. Ashmawy, A. Negm, L. A. Wessjohann, *Eur. J. Med. Chem.* **2019**, *179*, 515. (b)S. Shaaban, A. Negm, M. A. Sobh, L. A. Wessjohann, *Eur. J. Med. Chem.* **2015**, *97*, 190.

[47] (a)S. Shaaban, A. Negm, M. A. Sobh, L. A. Wessjohann, *Anti-Cancer Agents Med. Chem.* **2016**, *16*, 621. (b)S. Shaaban, A. Negm, A. M. Ashmawy, D. M. Ahmed, L. A. Wessjohann, *Eur. J. Med. Chem.* **2016**, *122*, 55.

[48] C. Martín-Cordero, M. López-Lázaro, M. Gálvez, M. Jesús Ayuso, *J. Enzyme Inhib. Med. Chem.* **2003**, *18*, 505.

[49] M. S. Blois, *Nature* **1958**, *29*, 1199.

[50] J. M. McCord, I. Fridovich, *J. Biol. Chem.* **1969**, *244*, 6049.

[51] (a)H. E. Gaffer, M. R. Elgohary, H. A. Etman, S. Shaaban, *Pigm. Resin Technol.* **2017**, *46*, 210. (b)S. Shaaban, F. Sasse, T. Burkholz, C. Jacob, *Bioorg. Med. Chem.* **2014**, *22*, 3610.

[52] (a)L. Shi, H. M. Ge, S. H. Tan, H. Q. Li, Y. C. Song, H. L. Zhu, R. X. Tan, *Eur. J. Med. Chem.* **2007**, *42*, 558. (b)C. M. Da Silva, D. L. da Silva, L. V. Modolo, R. B. Alves, M. A. de Resende, C. V. Martins, Â. de Fátima, *J. Adv. Res.* **2011**, *2*, 1.

[53] (a)M. Shebl, *Spectrochim. Acta a* **2014**, *117*, 127. (b)M. Shebl, S. M. E. Khalil, *Monatsh. Chem.* **2015**, *146*, 15. (c)M. Gaber, N. El-Wakiel, K. El-Baradie, S. Hafez, *J. Iran. Chem. Soc.* **2019**, *16*, 169.

[54] (a)H. M. Abd El-Lateef, M. S. S. Adam, M. M. Khalaf, *J. Taiwan Inst. Chem. Eng.* **2018**, *88*, 286. (b)T. G. Jo, J. J. Lee, E. Nam, K. H. Bok, M. H. Lim, C. Kim, *New J. Chem.* **2016**, *40*, 8918.

[55] (a)S. D. Kurbah, A. Kumar, I. Syiemlieh, R. A. Lal, *Polyhedron* **2018**, *139*, 80. (b)S. D. Kurbah, A. Kumar, O. S. Ozukum, I. Syiemlieh, R. A. Lal, *J. Coord. Chem.* **2017**, *70*, 2969.

[56] (a)M. Shebl, S. M. E. Khalil, A. Taha, M. A. N. Mahdi, *J. Mol. Struct.* **2012**, *1027*, 140. (b)M. Shebl, *Spectrochim. Acta a* **2008**, *70*, 850. (c)M. Shebl, H. S. Seleem, B. A. El-Shetary, *Spectrochim. Acta A* **2010**, *75*, 428. (d)H. S. Seleem, B. A. El-Shetary, S. M. E. Khalil, M. Mostafa, M. Shebl, *J. Coord. Chem.* **2005**, *58*, 479. (e)H. F. El-Shafiy, M. Shebl, *J. Mol. Struct.* **2018**, *1156*, 403.

[57] (a)M. Shebl, *Spectrochim. Acta a* **2009**, *73*, 313. (b)M. Shebl, S. M. E. Khalil, A. Taha, M. A. N. Mahdi, *Spectrochim. Acta A* **2013**, *113*, 356. (c)M. Shebl, S. M. E. Khalil, F. S. Al-Gohani, *J. Mol. Struct.* **2010**, *980*, 78. (d)M. Shebl, M. A. Ibrahim, S. M. E. Khalil, S. L. Stefan, H. Habib, *Spectrochim. Acta A* **2013**, *115*, 399. (e)H. F. El-Shafiy, M. Shebl, *J. Mol. Struct.* **2019**, *1194*, 187.

[58] (a)A. Golmohamadpour, B. Bahramian, A. Shafiee, L. Ma'mani, *Mater. Chem. Phys.* **2018**, *218*, 326. (b)M. Cindric, G. Pavlovic, R. Katava, D. Agustin, *New J. Chem.* **2017**, *41*, 594. (c)W. Wang, J.-C. Daran, R. Poli, D. Agustin, *J. Mol. Catal. A* **2016**, *416*, 117.
[59] (a)B. Gao, M. Wan, J. Men, Y. Zhang, *Appl. Catal. A* **2012**, *439*, 156. (b)S. D. Kurbah, A. Kumar, I. Syiemlieh, M. Asthana, R. A. Lal, *Inorg. Chem. Commun.* **2017**, *86*, 39.
[60] (a)A. Bezaatpour, E. Askarizadeh, S. Akbarpour, M. Amiria, B. Babaei, *Mol. Catal.* **2017**, *436*, 199. (b)R. Bikas, V. Lippolis, N. Noshiranzadeh, H. Farzaneh-Bonab, A. J. Blake, M. Siczek, H. Hosseini-Monfared, T. Lis, *Eur. J. Inorg. Chem.* **2017**, 999.
[61] L. H. Abdel-Rahman, A. M. Abu-Dief, M. S. S. Adam, S. K. Hamdan, *Catal. Lett.* **2016**, *146*, 1373.
[62] (a)M. S. S. Adam, A. M. Hafez, I. El-Ghamry, *Reac. Kinet. Mech. Cat.* **2018**, *124*, 779. (b)M. S. S. Adam, M. A. Al-Omair, F. Ullah, *Res. Chem. Intermediat.* **2019**, *45*, 4653.
[63] (a)F. Jalilian, B. Yadollahi, M. R. Farsani, S. Tangestaninejad, H. A. Rudbari, R. Habibi, *Cat. Com.* **2015**, *66*, 107. (b)A. Di Giuseppe, C. Di Nicola, R. Pettinari, I. Ferino, D. Meloni, M. Passacantando, M. Crucianelli, *Catal. Sci. Technol.* **2013**, *3*, 1972.
[64] (a)J. Adhikary, A. Datta, S. Dasgupta, A. Chakraborty, M. I. Menendez, T. Chattopadhyay, *RSC Adv.* **2015**, *5*, 92634. (b)S. A. Talouki, G. Grivani, A. D. Khalaji, *Appl. Organomet. Chem.* **2017**, *31*, e4078.
[65] (a)H. Sugimoto, H. Tano, H. Miyake, S. Itoh, *Dalton Trans.* **2011**, *40*, 2358. (b)R. Mayilmurugan, B. N. Harum, M. Volpe, A. F. Sax, M. Palaniandavar, N. C. Mçsch-Zanetti, *Chem. – Eur. J.* **2011**, *17*, 704.
[66] M. Khorshidifard, H. A. Rudbari, B. Askari, M. Sahihi, M. R. Farsani, F. Jalilian, G. Bruno, *Polyhedron* **2015**, *95*, 1.
[67] (a)S. Figueiredo, A. C. Gomes, J. A. Fernandes, F. A. Almeida Paz, A. D. Lopes, J. P. Lourenço, M. Pillinger, I. S. Gonçalves, *J. Organomet. Chem.* **2013**, *723*, 56. (b)C. Bibal, J.-C. Daran, S. Deroover, R. Poli, *Polyhedron* **2010**, *29*, 639.
[68] (a)S. Hazra, L. M. D. R. S. Martins, M. F. C. G. da Silva, A. J. L. Pombeiro, *RSC Adv.* **2015**, *5*, 90079. (b)E. Steves, S. S. Stahl, *J. Am. Chem. Soc.* **2013**, *135*, 15742. (c)E. Zueva, P. Walton, J. E. McGrady, *Dalton Trans.* **2006**, *1*, 159.
[69] L. G. M. Slaughter, J. P. Collman, T. A. Eberspacher, J. I. Brauman, *Inorg. Chem.* **2004**, *43*, 5198.
[70] M. Zare, Z. Moradi-Shoeili, *Appl. Organomet. Chem.* **2017**, *31*, e3611.
[71] M. Sarkheil, M. Lashanizadegan, *Appl. Organomet. Chem.* **2018**, *32*, e4459.
[72] A. Schmidt, N. Grover, T. K. Zimmermann, L. Graser, M. Cokoja, A. Pothig, F. E. Kühn, *J. Catal.* **2014**, *319*, 119.
[73] (a)C. Dinoi, M. Ciclosi, E. Manoury, L. Maron, L. Perrin, R. Poli, *Chem. – Eur. J.* **2010**, *16*, 9572. (b)M. M. Farahani, S. Shahsavarifar, *Appl. Organomet. Chem.* **2018**, *32*, e4064.
[74] S. Huang, F. Zhu, Q. Xiao, Y. Liang, Q. Zhou, W. Su, *RSC Adv.* **2015**, *5*, 42889.
[75] (a)X. L. Li, Y. J. Hu, H. Wang, B. Q. Yu, H. L. Yue, *Biomacromolecules* **2012**, *13*, 873. (b)R. Palchaudhuri, P. J. Hergenrother, *Curr. Opin. Biotechnol.* **2007**, *18*, 497.
[76] N. Shahabadi, S. Kashanian, F. Darabi, *Eur. J. Med. Chem.* **2010**, *45*, 4239.
[77] S. Terpilowska, A. K. Siwicki, *Chem.-Biol. Interact.* **2019**, *298*, 43.
[78] A. Palanimurugan, A. Dhanalakshmi, P. Selvapandian, A. Kulandaisamy, *Heliyon* **2019**, *5*, e02039.
[79] (a)M. Shebl, S. M. E. Khalil, S. A. Ahmed, H. A. A. Medien, *J. Mol. Struct.* **2010**, *980*, 39. (b)M. Shebl, M. Saif, A. I. Nabeel, R. Shokry, *J. Mol. Struct.* **2016**, *1118*, 335.
[80] R. Garg, N. Fahmi, R. V. Singh, *Russ. J. Coord. Chem.* **2008**, *34*, 198.
[81] A. Leite, L. J. Bessa, A. M. Silva, P. Gameiro, B. de Castro, M. Rangel, *J. Inorg. Biochem.* **2019**, *197*, 110704.

SUPPORTING INFORMATION

Additional supporting information may be found online in the Supporting Information section at the end of this article.

How to cite this article: Adam MSS, Ahmed MSM, El-Hady OM, Shaaban S. *Bis*-dioxomolybdenum (VI) oxalyldihydrazone complexes: Synthesis, characterization, DFT studies, catalytic epoxidation potential, molecular modeling and biological evaluations. *Appl Organometal Chem*. 2020;e5573. https://doi.org/10.1002/aoc.5573